Dynamics and Control of a Planar Truss Actuator

by

Vincent Dean Lovejoy

Thesis submitted to the Faculty of the

Virginia Polytechnic Institute and State University

in partial fulfillment of the requirements for the degree of

Master of Science

in

Mechanical Engineering

APPROVED:

Dr. Harry H. Robertshaw, Chairman

Dr. Robert G. Leonard

Dr. Robert H. Fries

April, 1987

Blacksburg, Virginia

Dynamics and Control of a Planar Truss Actuator

by

Vincent Dean Lovejoy

Dr. Harry H. Robertshaw, Chairman

Mechanical Engineering

(ABSTRACT)

Recent demands in large space structure technology have suggested the use of active control actuators integral to a structures' construction. The concept of an 3-D (triangular cross-sectioned) active truss is presented. The linear equations of motion for one plane of the truss are derived. A model for a generic flexible beam are then appended to the planar truss model. A linear time-invariant optimal control law is found, followed by a presentation of an experimental planar truss built to test the concept. Physical parameters are then substituted into the dynamic model and several sets of control gains are found. The "Kalman" gains are applied to the experimental structure. Experimental results are compared to expected theoretical results with good (30%) correlation. Conclusions are drawn and suggestions are made for further research.

Acknowledgements

I would like to take this bit of space to thank several of the people, without whom this work would not have been possible. First, thanks go out to all the people in the machine and instrumentation shops. This work truly would have been impossible without your help and patience.

I would also like to thank Dr. Leonard and Dr. Fries for serving on my committee. I would especially like to thank Dr. (Harry) Robertshaw for the hours of consulting and guidance he has given me, complaining he has had to endure and laughing that we went through together on the road to finishing this thesis.

My last thanks I have saved for the people in the background who have helped me maintain some semblance of sanity through this ordeal. In particular thank you:

and

It doesn't seem enough to just say it, but thank you Mom and Dad. I'll never be able to repay everything you've given me.

Table of Contents

List of Illustrations

List of Tables

List of Symbols

A_i	Mode shape weighting coefficients
B_i	Mode shape weighting coefficients
$\mathbf{B}_r$	Vector of beam reaction forces - R_x, R_y, M_r
$\mathbf{D}$	Gain set transformation matrix
$\mathbf{E}$	Vector of potentiometer readings
EI	Beam flexure rigidity
$\mathbf{F}$	Feedback gain matrix
G	Actuator lead screw gain
G_p	Potentiometer gain
$\mathbf{I}$	Identity Matrix
I_i	Ritz formulation beam integrals
$J_{i\varphi}$, J_{il}	Actuator inertia constants
$\mathbf{K}$	Solution vector to differential Ricatti equation
K_b	Motor back EMF constant
$\mathbf{K}_c$	Beam stiffness matrix
K_t	Motor torque constant
L	Length of beam
$\mathscr{L}$	System Lagrangian
$\mathbf{M}_b$	Overall actuator mass matrix
$\mathbf{M}_c$	Beam mass matrix
M_p, J_p	Link 4 mass and inertia
$\mathbf{M}_\varphi$, $\mathbf{M}_l$, $\mathbf{M}_{Pr}$	Actuator sub-mass matrices
$\mathbf{Pr}$	Vector of actuator coordinates - Z_x, Z_y, θ
$\mathbf{Pr}_0$	Actuator set point vector

Q, R, H	Linear quadratic regulator penalty matrices
$\overline{\mathbf{R}}$	Vector to differential beam element
R_a	Motor armature resistance
T_i	Kinetic energy terms
$\mathbf{T}_l$, $\mathbf{T}_\varphi$	Coodinate transformation matrices
V	Vector of motor input voltages - V_1, V_2, V_3
W	Work
a, b	State space system matrices
d	Fixed link length
f	Strain transition matrix
l	Vector of actuator coordinates - l_1, l_2, l_3
m_i	Link mass component
q	Vector of modal displacement coefficients - q_1, q_2, q_3
r_i	Link offset length
x	State space system coordinate vector
w	Beam displacement distance
y	Vector of system coordinates
$\boldsymbol{\varphi}$	Vector of actuator coordinates - φ_1, φ_2, φ_3
δ	Variational operator
θ_{mi}	Motor angular rotation
ξ	Beam's mass/unit length
γ_i	Mode shape weighting coefficients
λ	eigenvalue
$\boldsymbol{\varepsilon}$	Vector of strain readings
ζ	Damping ratio

1.0 Background of Research

1.1 Introduction

The current thrust in space technology has presented many demands on the engineering world. Growth in space will require lighter and stronger materials and designs. These demands, when placed on devices such as antennas, booms and solar arrays, will inherently produce very flexible structures. The task of controlling these structures through various loadings and articulations has received much attention lately. In fact, the National Aeronautics and Space Administration (NASA) has designed a Control of Flexible Structures (COFS) Flight Experiment Program to "systematically evaluate (control) algorithms and techniques ... for future NASA missions such as the evolutionary Space Station and large orbital antennas (1)."

Many concepts exist for controlling Large Space Structures (LSS). The most common, and most hopeful are active control devices. These devices are attached to, or built into the structure and use various control algorithms. One structure of intended use is a triangular cross-sectioned beam or truss. A single bay of such a structure is shown in Fig. 1. It may be used in structures such as appendages to Space Station, antennas and work platforms. This thesis presents the concept of an "active bay" for controlling such a structure. This active bay is then an inherent part of the structure, allowing control and articulation possibilities through movement of the six extensible links in each bay. As the research presented here is preliminary, a less complicated "planer actuator" is investigated first. The planer truss will provide a forum to test control algorithms, motor drivers,

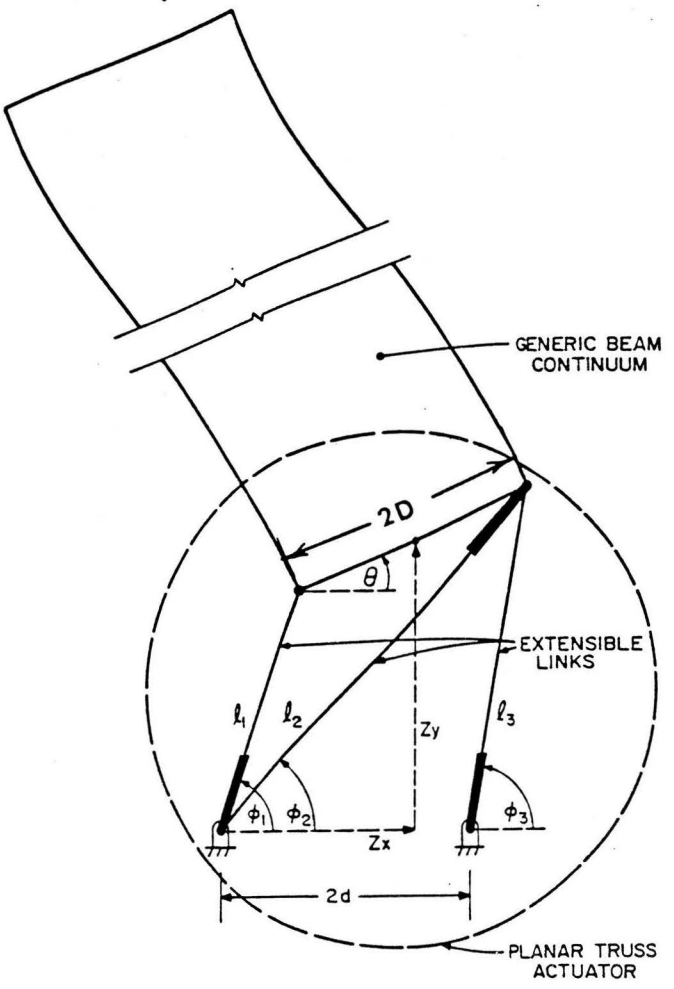

Figure 1. 3-Dimensional Active Bay

control formats (analog vs. digital) and any other variables in the task. The results from this research can then be extended to the three-dimensional active bay.

This report will then present the planer truss for control of a flexible structure. First the governing differential equations for a single bay of the planer actuator are developed. Next, the governing equations for a "generic" flexible structure are derived. This generic structure could represent some attachment to the bay controller or an continuation of the truss structure itself. In the later case the continuation of the structure might also include active bays, thereby allowing a larger range of mobility than allowed by one active bay. The two models are then added together forming a complete set of governing equations.

To demonstrate control of a flexible structure using the planer actuator, representative constants from an experimental test fixture constructed for this research are inserted into the model. A time-invariant optimal control law is then derived for the sample system. An analytical verification of the control law is then accomplished using eigenvalue techniques. The optimal control law is then applied to the experimental test fixture. Next, conclusions are drawn on the usefulness of this type of actuator, its advantages and disadvantages. Finally, recommendations of future research are made, including different modeling techniques and control algorithms, further testing on the planer model and extension to a three-dimensional active bay.

1.2 Literature Review

Large Space Structures (LSS) are generally defined as those structures designed for the near zero-g environment of space (1). This section presents a conceptual overview of Active Control of Space

Structures (ACOSS), including a summary of relevant research. Several challenges in ACOSS are also presented.

Control of LSS involves such tasks as: structure slewing, disturbance rejection, precision pointing and vibration damping. Kosut, et al. (2) present the most characteristic design objective for LSS controllers: "to guarantee performance and stability robustness in the presence of uncertain unmodeled dynamics." This objective is complicated by several characteristic problems (2,3):

1. Controlling an infinite dimensional system (structure continuum) with a finite dimensional controller.

2. Determining and compensating for the effects of actuator and sensor locations, number and dynamics.

3. Determining the effects of uncertain system parameters and unmodeled modes. Typically LSS have closely spaced modal frequencies.

4. Compensating for the effects of plant excitation.

5. Designing a controller with natural frequencies above major structural resonant frequencies to assure robustness.

Typically, a flexible spacecraft is modeled with a high-order model, such as finite elements. Although controller designs exist, in theory, for such models, implementation is limited due to computational delays, sensor and actuator numbers and locations. Several solutions to this problem exist, including frequency truncation, modal cost analysis, and singular value decomposition (2). According to Nurre, et al. (3), the model size and complexity is a function of the structure's per-

formance requirements and not the structure configuration. With the overall goals and problems of ACOSS described, attention is now turned to control actuators.

Several different actuator concepts exist to achieve ACOSS goals including reaction (momentum exchange) wheels and proof masses. McClamroch (4) presents a general discussion on ACOSS, for these force and moment force transducers, detailing their dynamic (vibration) effects on the flexible structure and the structure's effects on the actuators. His linear model analysis considers the actuators as force and moment inputs. Several examples of these theoretical and experimental member dampers are now presented, followed by a summary of relevant research for ACOSS using the truss actuator concept.

Reaction, or momentum exchange, wheels probably form the most tested group of ACOSS actuators. This closed-loop gyroscope type device exerts a moment on the controlled structure. Johnson (5) presents an analysis of this actuator with special attention given to analyzing its out-of-plane deflection. Johnson cites several simulations verifying control.

The proof mass actuator operates on much the same principle as dynamic vibration absorbers. A mass is accelerated back and forth with such devices as DC motors, stepper motors and solenoids to provide a linear force at the point of actuator installation. The actuator is controlled externally, either by analog or digital means. Mills (6) presents a theoretical comparison study between proof masses and reaction wheels. Experimental verification for proof mass actuators is provided by Zimmerman, et al. (7).

Juang (8) presents a control analysis using a single motor to apply a root torque to a flexible structure. He demonstrates good control ability. In many ways, then, the actuator concept pre-

sented here is an extension of Juang's work. The planer truss actuator will be able to apply a root torque as well as forces.

The truss actuator to be considered here is a combination of the proof mass and reaction wheel concept, providing both force and moment inputs to the system. The concept implements the actuator within the structure (at the root for this preliminary research), thereby combining its articulating device with the control. To date, all relevant research on truss actuators has been conducted on a test fixture constructed by the TRW Space and Technology Group in Redondo Beach, California. The structure simulates a single bay of an optics structure. It is square cross-sectioned, and uses one active link per side (i.e. the vertical links in Fig. 1 are rigid). The structure also incorporates passive damping elements. Major and Simonian (9) and Opdenacker, et al. (10) use differing control strategies on this fixture to attain the same goal of vibration disturbance rejection from external excitation devices. Note also that they only seek to control the vibration of a the control bay. No flexible structure is attached to the actuator. Since the structure is near rigid, deflections are limited to 1 - 2 mm. Consideration is also given to the optimal combination of passive and active dampers.

1.3 Motivation for this Work

With the previous mentioned information, the question then remains: "How is this research unique (and similar) and valuable to the field of ACOSS?" Several possible advantages of the truss actuator exist. First, the in-line actuator principle does not require extraneous masses as do the reaction wheels and proof masses. This benefit is obvious since the structure must be launched into space. Also note that (contrary to the TRW structure) large actuator motions are possible. Several active bays can be alternated with fixed bays to form a truss with extremely large excursion possibilities (eg. large curves, spirals, etc.). This actuator then presents many useful possibilities.

2.0 Derivation of System Equations of Motion

2.1 Overview of System Derivation

A schematic diagram of the planer truss actuator and a "generic" beam continuum are shown in Fig. 2. This continuum represents the remainder of the (truss-type) structure with fixed elements. Note that the actuator is a five link mechanism. Link 5 is ground. Link 4 is the articulating top plate, and links 1, 2 and 3 are the extensible controlling links. This section presents an overview of the derivation of equations of motion for the system. These equations will later be used to derive control laws for the system and to simulate the system response.

A variational approach is be taken to derive the actuator and beam continuum equations of motion independently. The independent derivations facilitates use of alternate flexible structures without rederivation of the actuator equations. Expressions for the kinetic and potential energies are first written; then, Lagrange's equations are applied with the generalized force inputs of the motors and beam reactions to form a set of differential equations. The beam equations are derived using a three-mode Ritz approximation to the beam continuum. The two governing sets of differential equations are then combined to form a set of system equations.

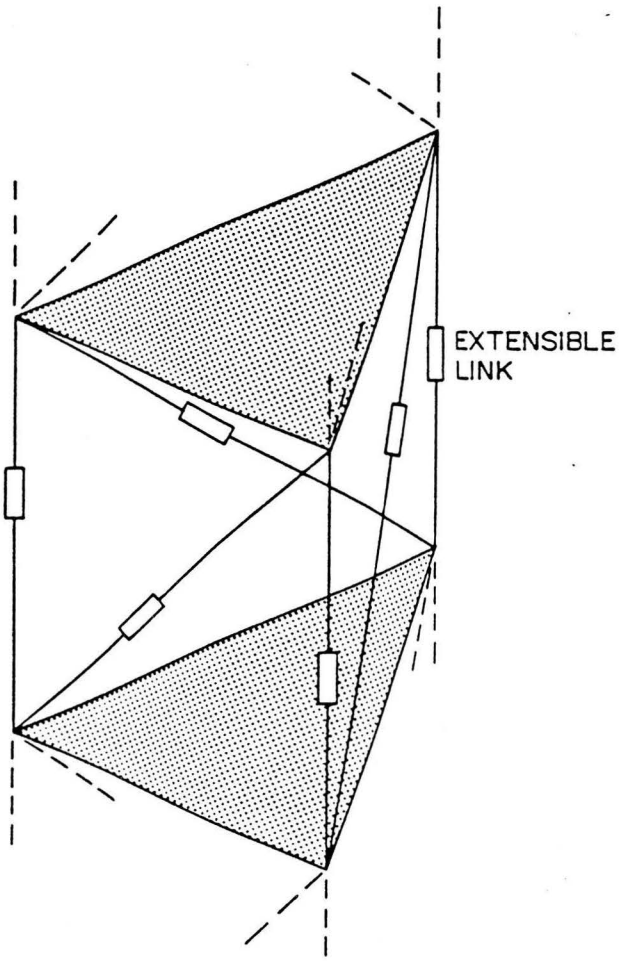

Figure 2. Planar Truss Actuator Schematic

2.2 Actuator Equations

This section presents a derivation of the equations of motion for the planer actuator (Fig. 2). An expression for the kinetic energy of the actuator is first written and the Lagrangian is formed. A lumped-mass approach will be used for the stiff actuator.

For simplicity it is convenient to dissect the actuator into individual links, write the energies for each, and then sum them. It can be shown that the kinetic energy (T) for links 1, 2 and 3 are:

$$T_i = \frac{1}{2}\left(J_{i\varphi} + m_i (l_i - r_i)^2 \right) \dot{\varphi}_i^2 + \frac{1}{2} J_{il} \dot{l}_i^2 \qquad : i = 1, 2, 3 \qquad [2.1]$$

The energy for link 4 can then be written as:

$$T_4 = \frac{1}{2} M_p (\dot{Z}_x^2 + \dot{Z}_y^2) + \frac{1}{2} J_p \dot{\theta}^2 \qquad [2.2]$$

As there is no significant potential energy storage mechanism in the actuator ($V = 0$) the Lagrangian ($\mathscr{L} = T - V$) can be written as:

$$\mathscr{L} = \dot{\boldsymbol{\varphi}}^t \mathbf{M}_{\varphi} \dot{\boldsymbol{\varphi}} + \dot{\mathbf{l}}^t \mathbf{M}_{l} \dot{\mathbf{l}} + \dot{\mathbf{Pr}}^t \mathbf{M}_{Pr} \dot{\mathbf{Pr}} \qquad [2.3]$$

Note that the Lagrangian is expressed in three different, but dependant, coordinate systems; therefore, it is necessary to introduce coordinate transformations that will allow the Lagrangian to be expressed in one system basis. The primitive system, **Pr**, ($[Z_x \; Z_y \; \theta]^t$) was chosen as the basis for convenience.

First a transformation from the **l**-coordinate system ($[l_1 \; l_2 \; l_3]^t$) to the primitives will be presented. Referring to Fig. 2, it can be shown that the **l** system relates to the primitives by:

$$l_1^2 = (Z_x - d\cos\theta)^2 + (Z_y - d\sin\theta)^2$$

$$l_2^2 = (Z_x + d\cos\theta)^2 + (Z_y + d\sin\theta)^2 \qquad [2.4]$$

$$l_3^2 = (Z_x + d\cos\theta - 2d)^2 + (Z_y + d\sin\theta)^2$$

Applying the δ-variational operator to both sides of the above equations, results in:

$$\delta \mathbf{l} = \mathbf{T}_l \, \delta \mathbf{Pr} \qquad [2.5]$$

where $\mathbf{T}_l$ is:

$$\begin{bmatrix} \dfrac{Z_x - d\cos\theta}{l_1} & \dfrac{Z_y - d\sin\theta}{l_1} & \dfrac{Z_x\, d\sin\theta - Z_y\, d\cos\theta}{l_1} \\ \dfrac{Z_x + d\cos\theta}{l_2} & \dfrac{Z_y + d\sin\theta}{l_2} & \dfrac{Z_y\, d\cos\theta - Z_x\, d\sin\theta}{l_2} \\ \dfrac{Z_x + d\cos\theta - 2d}{l_3} & \dfrac{Z_y + d\sin\theta}{l_3} & \dfrac{Z_y\, d\cos\theta - Z_x\, d\sin\theta + 2d^2\,\sin\theta}{l_3} \end{bmatrix}$$

As the variational and derivative operators have the same properties, Eq. 2.5 can also be written as:

$$\dot{\mathbf{l}} = \mathbf{T}_l \dot{\mathbf{Pr}} \qquad [2.6]$$

Next, a transformation from the φ coordinates ($[\varphi_1 \;\; \varphi_2 \;\; \varphi_3]^t$) to the primitive coordinates will be presented. Referring to Fig. 2, note that the following trigonometric equations can be written:

$$\cos\varphi_1 = \frac{1}{l_1}(Z_x - d\cos\theta)$$

$$\cos\varphi_2 = \frac{1}{l_2}(Z_x + d\cos\theta) \qquad [2.7]$$

$$\cos\varphi_3 = \frac{1}{l_3}(Z_x + d\cos\theta - 2d)$$

Substituting for l_1, l_2, l_3 from Eq. 2.4, and applying the δ-variational operator to both sides of the above equations leads to the transformation:

$$\delta\boldsymbol{\varphi} = \mathbf{T}_{\varphi}\,\delta\mathbf{Pr} \qquad [2.8]$$

where $\mathbf{T}_{\varphi}$ is:

$$\begin{bmatrix} \dfrac{-(Z_y - d\sin\theta)}{l_1^2} & \dfrac{-(Z_x - d\cos\theta)}{l_1^2} & \dfrac{-(Z_x - d\cos\theta)\,d\cos\theta - (Z_y - d\sin\theta)\,d\sin\theta}{l_1^2} \\ \dfrac{-(Z_y + d\sin\theta)}{l_2^2} & \dfrac{-(Z_x + d\cos\theta)}{l_2^2} & \dfrac{(Z_y + d\sin\theta)\,d\sin\theta + (Z_x + d\cos\theta)\,d\cos\theta}{l_2^2} \\ \dfrac{-(Z_y + d\sin\theta)}{l_3^2} & \dfrac{-(Z_x + d\cos\theta - 2d)}{l_3^2} & \dfrac{(Z_y + d\sin\theta)\,d\sin\theta + (Z_x + d\cos\theta - 2d)\,d\cos\theta}{l_3^2} \end{bmatrix}$$

Again, the transformation can be expressed in velocities:

$$\dot{\boldsymbol{\varphi}} = \mathbf{T}_{\varphi}\,\dot{\mathbf{Pr}} \qquad [2.9]$$

The Lagrangian for the actuator, Eq. 2.3, can now be rewritten by applying the two derived transformations (Eqs. 2.6 and 2.9).

$$\mathscr{L} = \dot{\mathbf{Pr}}^t\,\mathbf{M}_b\,\dot{\mathbf{Pr}} \qquad [2.10]$$

where:

$$\mathbf{M}_b = (\mathbf{T}_\varphi^t \mathbf{M}_\varphi \mathbf{T}_\varphi + \mathbf{T}_l^t \mathbf{M}_l \mathbf{T}_l + \mathbf{M}_{\mathrm{Pr}})$$

At this point a bi-linearization of the Lagrangian is introduced. The actuator is assumed to operate with small deflections about some arbitrary set point as $\mathbf{Pr}_0$. This bi-linearization amounts to defining $\mathbf{M}_b$ to be a constant. This restricts both transformations, $\mathbf{T}_\varphi$ and $\mathbf{T}_l$, and $\mathbf{M}_\varphi$ to be constants. Lagrange's equations are now presented as (11):

$$\frac{\mathrm{d}}{\mathrm{d}t}\left[\frac{\partial \mathscr{L}}{\partial \dot{x}_i}\right] - \frac{\partial \mathscr{L}}{\partial x_i} = D_i \qquad [2.11]$$

where x_i represents each of the generalized coordianates and D_i represents each of the generalized force inputs. The generalized forces can be found from the virtual work of the applied forces on the active truss.

$$\delta W = \mathbf{B}_r^t \cdot \delta \mathbf{Pr} + \mathbf{F}^t \cdot \delta \mathbf{l} \quad = (\mathbf{B}_r^t + \mathbf{F}^t \mathbf{T}_l) \cdot \delta \mathbf{Pr} \quad = \mathbf{D}^t \cdot \delta \mathbf{Pr} \qquad [2.12]$$

where $\mathbf{B}_r$ represents reaction forces from the beam and $\mathbf{F}$ represents force inputs from the three motors. So that:

$$\mathbf{D} = \mathbf{B}_r + \mathbf{T}_l^t \mathbf{F} \qquad [2.13]$$

Applying Lagrange's equations to Eq. 2.10, yields the equations of motion for the acuator:

$$2\mathbf{M}_b \ddot{\mathbf{Pr}} = \mathbf{B}_r + \mathbf{T}_l \mathbf{F} \qquad [2.14]$$

An appropriate model for the motor will now be introduced. Torque for a dc armature-controlled motor (neglecting inductance effects) can be modeled as:

$$T_i = \frac{K_T}{R_a}(V_i - K_B \dot{\theta}_{mi}) \qquad [2.15]$$

where V_i is the input voltage and $\dot{\theta}_{mi}$ is the motor's rotational speed.

Incorporating the actuators lead-screw gain (G), $\mathbf{F}$ in Eq. 2.14 can be replaced by Eq. 2.15, yielding a final form for the actuator's equations of motion:

$$2\,\mathbf{M}_b\,\ddot{\mathbf{Pr}} + \frac{K_T K_b}{G^2 R_a}\mathbf{T}_l^t\,\mathbf{T}_l\,\dot{\mathbf{Pr}} = \mathbf{B}_r + \frac{K_T}{G R_a}\mathbf{T}_l^t\,\mathbf{V} \qquad [2.16]$$

where $\mathbf{V}$ represents the vector of motor input voltages. Note that the introduction of the motor model adds a damping term to the second order model. Next a derivation of the beam equations of motion will be presented.

2.3 Beam Equations

The potential and kinetic energies for the beam will be written using a three-mode Ritz approximation for the beam. Lagrange's equations are then applied to form a set of governing equations.

Figure 3 shows a schematic of the beam to be modeled. The kinetic energy of the beam can be found by locating a differential element of mass along the beam with a vector $\overline{\mathbf{R}}$:

$$\overline{\mathbf{R}} = (Z_x - x\sin\theta - w\cos\theta)\,\mathbf{i} + (Z_y + x\cos\theta - w\sin\theta)\,\mathbf{j} \qquad [2.17]$$

The kinetic energy for the beam can then be formed from the equation:

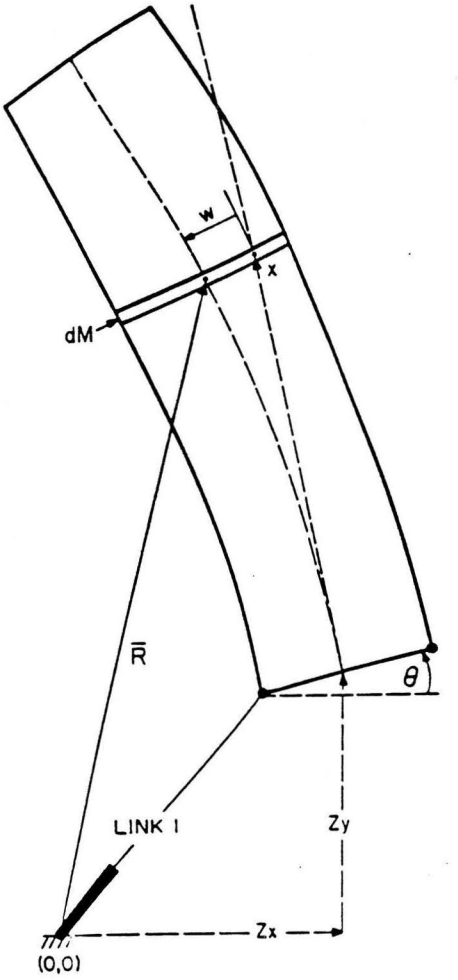

Figure 3. Generic Beam Continuum Schematic

$$T = \frac{1}{2}\int_m (\dot{\bar{\mathbf{R}}} \cdot \dot{\bar{\mathbf{R}}})\, dm = \frac{\xi}{2}\int^L (\dot{\bar{\mathbf{R}}} \cdot \dot{\bar{\mathbf{R}}})\, dx \qquad [2.18]$$

where ξ is the beam's mass/unit length and L is the length of the beam. An expression for $\dot{\bar{\mathbf{R}}} \cdot \dot{\bar{\mathbf{R}}}$ is then formed by taking the time derivative of Eq. 2.17 and dropping any $\dot{x}$ terms (assuming the beam is inextensible). This is then substituted into Eq. 2.18 and integrated, yielding:

$$\begin{aligned} T = \frac{\xi}{2}(&\dot{Z}_x^2 L + \dot{Z}_y^2 L + \frac{L^3}{3}\dot{\theta}^2 + \int^L \dot{w}^2\, dx + \dot{\theta}^2 \int^L w^2\, dx + 2\dot{\theta}\int^L x\dot{w}\, dx \\ &- L^2\dot{\theta}\,(\dot{Z}_x \cos\theta + \dot{Z}_y \sin\theta) - 2(\dot{Z}_x \cos\theta + \dot{Z}_y \sin\theta)\int^L \dot{w}\, dx \\ &+ 2\dot{\theta}\,(\dot{Z}_x \sin\theta - \dot{Z}_y \cos\theta)\int^L w\, dx) \end{aligned} \qquad [2.19]$$

Note the existence of several unevaluated integrals. The Ritz approximation to the beam continuum allows these integrals to be evaluated. The approximation involves a summation of assumed mode shapes for the structure:

$$w(x,t) = \sum_{i=1}^{n} \varphi_i(x)\, q_i(t) \qquad [2.20]$$

where φ_i represents the assumed individual mode shapes and q_i represents the modal coefficients.

The first three normalized (to 1.0 m end deflection) mode shapes for a clamped-free beam: φ_1, φ_2, φ_3 are used in this model. Figure 4 shows a representation of these mode shapes.

$$\varphi_i(x) = A_i[\cosh\beta_i x - \gamma_i \sinh\beta_i x - \cos\beta_i x + \gamma_i \sin\beta_i x] \qquad [2.21]$$

where Table 1 defines the constants in Eq. 2.21.

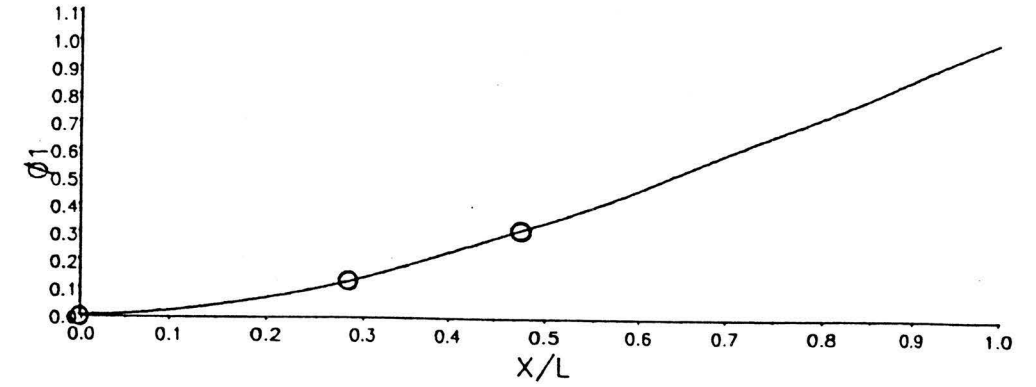

a) First Mode

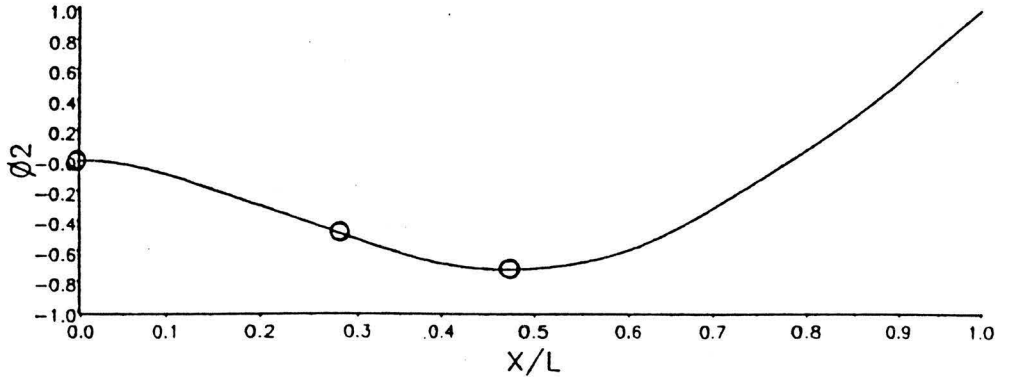

b) Second Mode

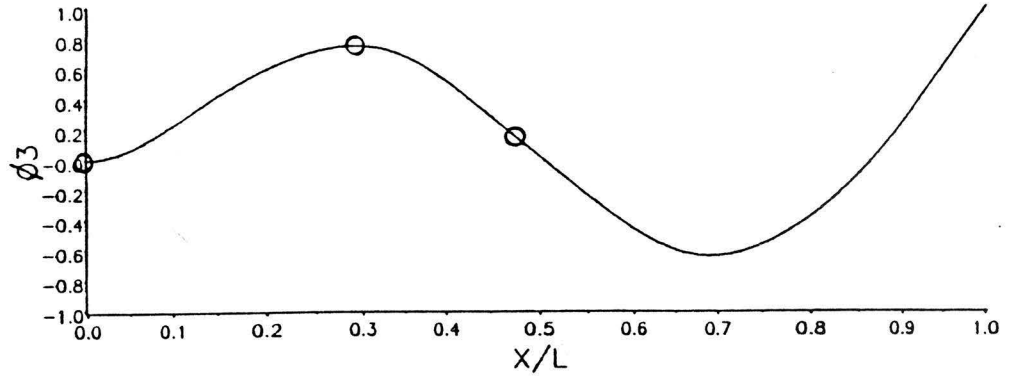

c) Third Mode

Figure 4. Bending Modes for a Cantelivered Beam

i	A_i	γ_i	$L \cdot \beta_i$
1	0.5	0.7348	1.8762
2	-0.5	1.0186	4.6904
3	0.4921	0.9992	7.8549

Table 1. Clamped-free Ritz parameters

After substituting Eq. 2.20 into Eq. 2.19, the remaining integrals are evaluated numerically. The final kinetic energy for the beam can then be written as:

$$\begin{aligned} T = \frac{\xi}{2}(& \dot{Z}_x^2 L + \dot{Z}_y^2 L + \frac{L^3}{3}\dot{\theta}^2 + \dot{q}_1^2 I_4 + \dot{q}_2^2 I_5 + \dot{q}_3^2 I_6 + \dot{q}_1 \dot{q}_2 I_7 + \dot{q}_1 \dot{q}_3 I_8 \\ & + \dot{q}_2 \dot{q}_3 I_9 + \dot{\theta}^2 (q_1^2 I_4 + q_2^2 I_5 + q_3^2 I_6 + q_1 q_2 I_7 + q_1 q_3 I_8 + q_3 q_3 I_9) \\ & + 2\dot{\theta} (I_{10} \dot{q}_1 + I_{11} \dot{q}_2 + I_{12} \dot{q}_3) - L^2 \dot{\theta} (\dot{Z}_x \cos\theta + \dot{Z}_y \sin\theta) \\ & - 2(\dot{Z}_x \cos\theta + \dot{Z}_y \sin\theta)(\dot{q}_1 I_1 + \dot{q}_2 I_2 + \dot{q}_3 I_3) \\ & + 2\dot{\theta} (\dot{Z}_x \sin\theta - \dot{Z}_y \cos\theta)(q_1 I_1 + q_2 I_2 + q_3 I_3)) \end{aligned} \qquad [2.22]$$

where the I_i represent integrals of the mode shapes.

Next the potential energy of the beam is written. Since the beam's only energy storage mechanism is strain, the potential energy is written as strain energy.

$$V = \frac{EI}{2} \int^L [w''(x)]^2 \, dx \qquad [2.23]$$

where E represents Young's modulus and I is the beam's area moment of inertia. Again, substituting the Ritz approximation (Eq. 2.20) and evaluating (Eq. 2.23) leads to:

$$V = \frac{EI}{2} (q_1^2 I_{13} + q_2^2 I_{14} + q_3^2 I_{15} + q_1 q_2 I_{16} + q_1 q_3 I_{17} + q_2 q_3 I_{18}) \qquad [2.24]$$

The definitions for all the integrals, I_i, are given in appendix A.

Next the Lagrangian is formed and Lagrange's equations, Eq. 2.11, are applied. The non-linear beam equations are then presented as:

$$\begin{aligned}\frac{\xi}{2}(2\ddot{Z}_x L - L^2\ddot{\theta}\ \cos\theta + L^2\dot{\theta}^2\sin\theta - 2\cos\theta(\ddot{q}_1 I_1 + \ddot{q}_2 I_2 + \ddot{q}_3 I_3) \\ + 4\dot{\theta}\sin\theta(\dot{q}_1 I_1 + \dot{q}_2 I_2 + \dot{q}_3 I_3) \\ + 2(\dot{\theta}^2\cos\theta + \ddot{\theta}\ \sin\theta)(q_1 I_1 + q_2 I_2 + q_3 I_3)) = -R_x\end{aligned} \qquad [2.25]$$

$$\begin{aligned}\frac{\xi}{2}(2\ddot{Z}_y L - L^2\ddot{\theta}\ \sin\theta - L^2\dot{\theta}^2\cos\theta - 2\sin\theta(\ddot{q}_1 I_1 + \ddot{q}_2 I_2 + \ddot{q}_3 I_3) \\ - 4\dot{\theta}\cos\theta(\dot{q}_1 I_1 + \dot{q}_2 I_2 + \dot{q}_3 I_3) \\ + 2(\dot{\theta}^2\sin\theta - \ddot{\theta}\ \cos\theta)(q_1 I_1 + q_2 I_2 + q_3 I_3)) = -R_y\end{aligned}$$

$$\begin{aligned}&\frac{\xi}{2}(\frac{2}{3}L^3\theta + 2\ddot{\theta}\ (q_1^2 I_4 + q_2^2 I_5 + q_3^2 I_6 + q_1 q_2 I_7 + q_1 q_3 I_8 + q_2 q_3 I_9) \\ &+ 2\dot{\theta}\ (2 q_1\dot{q}_1 I_4 + 2 q_2\dot{q}_2 I_5 + 2 q_3\dot{q}_3 I_6 + I_7(\dot{q}_1 q_2) + I_8(\dot{q}_1 q_3) + I_9(\dot{q}_2 q_3)) \\ &+ 2(I_{10}\ddot{q}_1 + I_{11}\ddot{q}_2 + I_{12}\ddot{q}_3) - L^2(\ddot{Z}_x\cos\theta + \ddot{Z}_y\sin\theta) \\ &+ 2(\ddot{Z}_x\sin\theta - \ddot{Z}_y\cos\theta)(q_1 I_1 + q_2 I_2 + q_3 I_3)) = -M_r\end{aligned}$$

$$\begin{aligned}&\frac{\xi}{2}(2 I_4\ddot{q}_1 + I_7\ddot{q}_2 + I_8\ddot{q}_3 + 2 I_{10}\ddot{\theta}\ - 2 I_1(\ddot{Z}_x\cos\theta + \ddot{Z}_y\sin\theta) \\ &- \dot{\theta}^2(2 I_4 q_1 + I_7 q_2 + I_8 q_3)) + \frac{EI}{2}[2 q_1 I_{13} + I_{16} q_2 + I_{17} q_3] = 0\end{aligned}$$

$$\begin{aligned}&\frac{\xi}{2}(2 I_5\ddot{q}_2 + I_7\ddot{q}_1 + I_9\ddot{q}_3 + 2 I_{11}\ddot{\theta}\ - 2 I_2(\ddot{Z}_x\cos\theta + \ddot{Z}_y\sin\theta) \\ &- \dot{\theta}^2(2 I_5 q_2 + I_7 q_1 + I_9 q_3)) + \frac{EI}{2}(2 q_2 I_{14} + I_{16} q_1 + I_{18} q_3) = 0\end{aligned}$$

$$\frac{\xi}{2}(2 I_6 \ddot{q}_3 + I_8 \ddot{q}_1 + I_9 \ddot{q}_2 + 2 I_{12} \ddot{\theta} - 2 I_3 (\ddot{Z}_x \cos\theta + \ddot{Z}_y \sin\theta)$$
$$- \dot{\theta}^2 (2 I_6 q_3 + I_8 q_1 + I_9 q_2)) + \frac{EI}{2} (2 q_3 I_{15} + I_{17} q_1 + I_{18} q_2) = 0$$

where R_x, R_y, and M_r represent the force inputs at the root of the beam due to the actuator. Similar to the actuator equations, these equations can be linearized about a point $\mathbf{Pr}_0$ to give:

$$\mathbf{M}_c \ddot{\mathbf{y}} + \mathbf{K}_c \mathbf{y} = - \mathbf{B}_r \qquad [2.26]$$

where:

$$\mathbf{M}_c = \begin{bmatrix} \xi L & 0 & -\frac{\xi}{2} L^2 & -\xi I_1 & -\xi I_2 & -\xi I_3 \\ 0 & \xi L & 0 & 0 & 0 & 0 \\ -\frac{\xi}{2} L^2 & 0 & \xi \frac{L^3}{3} & \xi I_{10} & \xi I_{11} & \xi I_{12} \\ -\xi I_1 & 0 & \xi I_{10} & \xi I_4 & \frac{\xi}{2} I_7 & \frac{\xi}{2} I_8 \\ -\xi I_2 & 0 & \xi I_{11} & \frac{\xi}{2} I_7 & \xi I_5 & \frac{\xi}{2} I_9 \\ -\xi I_3 & 0 & \xi I_{12} & \frac{\xi}{2} I_8 & \frac{\xi}{2} I_9 & \xi I_6 \end{bmatrix}$$

$$\mathbf{K}_c = \begin{bmatrix} 0 & 0 & 0 & 0 & 0 & 0 \\ 0 & 0 & 0 & 0 & 0 & 0 \\ 0 & 0 & 0 & 0 & 0 & 0 \\ 0 & 0 & 0 & EI\, I_{13} & \frac{EI}{2} I_{16} & \frac{EI}{2} I_{17} \\ 0 & 0 & 0 & \frac{EI}{2} I_{16} & EI\, I_{14} & \frac{EI}{2} I_{18} \\ 0 & 0 & 0 & \frac{EI}{2} I_{17} & \frac{EI}{2} I_{18} & EI\, I_{15} \end{bmatrix}$$

$$\mathbf{y} = \begin{bmatrix} Z_x & Z_y & \theta & q_1 & q_2 & q_3 \end{bmatrix}^t$$

$$\mathbf{B}_r = \begin{bmatrix} R_x & R_y & M_r & 0 & 0 & 0 \end{bmatrix}^t$$

2.4 Combination of the Models

The final step in the derivation of the total system equations of motion is to augment the actuator equations (Eq. 2.16), with an appropriate number of rows and columns to include $q_1 - q_3$ as state vectors and add them to the generic beam equations (Eq. 2.26), yielding:

$$[\, 2\,\mathbf{M}_b + \mathbf{M}_c \,]\,\ddot{\mathbf{y}} + \left[\frac{K_T K_b}{G^2 R_a} \mathbf{T}_l^t \mathbf{T}_l \right] \dot{\mathbf{y}} + \mathbf{K}_c \mathbf{y} = \frac{K_T}{G R_a} \mathbf{T}_l^t \mathbf{V} \qquad [2.27]$$

3.0 Control Law Development

This chapter presents a background and derivation for the optimal control law that will be used to control the planer actuator. This control law is known as the linear quadratic regulator (LQR) and its development is attributed primarily to R.E. Kalman. It will be shown that for the linear class of problems, the optimal control is a time-varying function of the system states (12). Under certain conditions, it can be shown that this function is time-invariant, forming a set of "Kalman" gains. These Kalman gains will form the control law for the planer actuator.

The system equations described in Eq. 2.27 can be written in a standard state-space format:

$$\dot{\mathbf{x}} = \mathbf{a}\,\mathbf{x} + \mathbf{b}\,\mathbf{V} \qquad [3.1]$$

where:

$$\mathbf{x} = \begin{bmatrix} \mathbf{y} \\ \dot{\mathbf{y}} \end{bmatrix} \qquad [3.2]$$

The standard performance measure for the LQR problem is:

$$J = \frac{1}{2}\mathbf{x}^t(t_f)\,\mathbf{H}\,\mathbf{x}(t_f) + \frac{1}{2}\int_{t_0}^{t_f} [\,\mathbf{x}^t\,\mathbf{Q}\,\mathbf{x} + \mathbf{u}^t\,\mathbf{R}\,\mathbf{u}\,]\;dt \qquad [3.3]$$

where the final time, t_f is fixed, **Q**, **R**, **H** are weighting matrices, and **u** is the generalized control vector. This performance measure can be said to "... maintain the state vector close to the origin without excessive expenditure of control effort" (12).

Applying variational techniques, it can be shown that the optimal control is of the form:

$$\mathbf{u} = -\mathbf{R}^{-1}\mathbf{b}^t\mathbf{K}\mathbf{x} = -\mathbf{F}\mathbf{x} \qquad [3.4]$$

where $\mathbf{K}$ is the $n \times n$ solution matrix to the problems Ricatti differential equation:

$$\dot{\mathbf{K}} = -\mathbf{K}\mathbf{a} - \mathbf{a}^t\mathbf{K} - \mathbf{Q} + \mathbf{K}\mathbf{b}\mathbf{R}^t\mathbf{K} \qquad [3.5]$$

with the associated boundary condition: $\mathbf{K}(t_f) = \mathbf{H}$.

Note that the solution to the matrix Ricatti equation leads to a time varying control input, $\mathbf{u}$, since $\mathbf{K}$ is time-varying.

Consider the case where the system to be controlled is of an infinite time duration. Kalman (13) has shown that if (1) the plant is completely controllable, (2) $\mathbf{H} = \mathbf{0}$, and (3) $\mathbf{a}$, $\mathbf{b}$, $\mathbf{Q}$, and $\mathbf{R}$ are constant matrices then $\mathbf{K}$ approaches a constant matrix as $t_f \rightarrow \infty$. $\mathbf{F}$ in Eq. 3.4 is then constant and termed the set of Kalman gains. The Kalman gains are solved for by setting $\dot{\mathbf{K}}$ in the Ricatti equation to zero and solving the non-linear set of algebraic equations. Several numerical solution methods exist for this type of problem. Potter's method (14) was used here.

The time-invariant Kalman gains set will be used to control the planer truss actuator. This method presents several advantages over the time-varying optimal gain solution. The Kalman gains are much easier to realize physically. Several analog amplifiers with preset gains can be used whereas for the time-varying solution complicated function generation must be used or control must be effected with a digital computer. Since digital control of a system adds further complexity to the

control problem, the time-invariant method was selected. In addition, the structure to be controlled potentially has continuous disturbance inputs, requiring an infinite time controller.

4.0 Experimentation

To demonstrate effective control using the planer truss actuator, an experimental test stand was constructed. This section will present the stand and its associated electrical hardware. The characteristics of the actuator and beam will then be used to form a set of system equations according to the derivation presented in Chapter 2. After a brief discussion of system characteristics, the set of equations will be used to define two Kalman gain sets according to the optimal control law presented in Chapter 3. After a transformation of states, these gain sets are applied to the actuator. Time responses for each gain set are then presented, for later comparison with expected analytical responses.

4.1 Experimental Apparatus and Instrumentation

Figure 5 shows the experimental planer actuator with an attached cantilevered beam. The actuator is constructed almost entirely of plate aluminum. Links 1, 2, and 3 (Fig. 2) are extensible via a motor and ball-screw combination. The DC motors are geared internally and connected to the ball-screws through a thrust bearing arrangement. Attached to each extensible link is a 0.305 m (12 in.) stroke linear potentiometer. The maximum stroke of each link is then slightly less than 0.305 m (12 in.), due to mounting requirements.

Figure 5. Experimental Planer Truss Actuator

The beam, supplied by Associated Spring Inc., is made of spring steel and is 1.016 m long. Attached to the beam are three sets of strain gages. The positioning of these gages is shown in Fig. 4 (by small circles). From the bending strain measured by these gages, the modal displacement coefficients can be inferred. The signal from each strain gage is then fed into a strain gage bridge amplifier.

Figure 6 shows the instrumentation and supporting electrical hardware for the truss actuator test stand. The two EAI TR-20 analog computers form the heart of the control system. Signals are input to the computers from the linear potentiometers and the strain gage bridge amplifiers. The control law is then formed on the analog computers and output to the motor driver amplifiers. The strip-chart recorder is used for documentation. A more detailed description of system components is given in Appendix A.

4.2 Model Assembly and Analysis

Next, a specific model for the experimental truss must be developed. Data from Appendix A is inserted into the equations derived in Chapter 2. The resulting set of equations presented in Appendix B is of the form:

$$\mathbf{M}\ddot{\mathbf{y}} + \mathbf{C}\dot{\mathbf{y}} + \mathbf{K}\mathbf{y} = \mathbf{B}\mathbf{V} \qquad [4.1]$$

At this point, we examine the actuator's open-loop eigenvalues. Transforming Eq. 4.1 to state space format (Eq. 3.1) allows determination of the eigenvalues by solution of:

$$(\mathbf{a} - \lambda \mathbf{I})\,\mathbf{x} = \mathbf{0} \qquad [4.2]$$

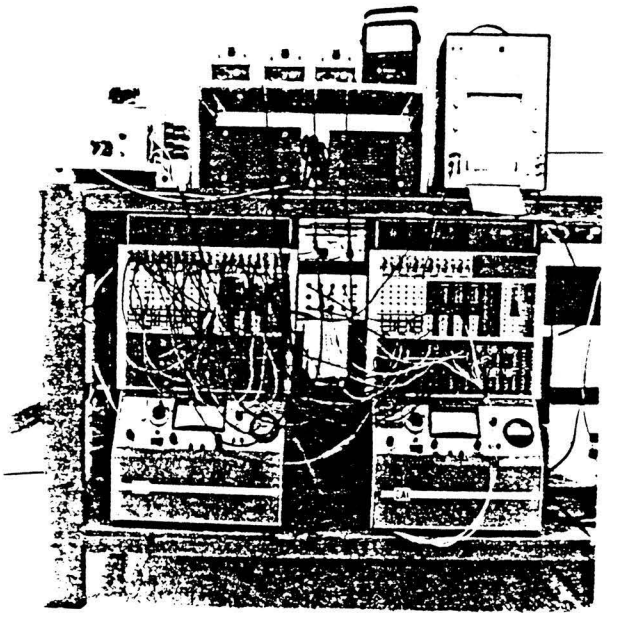

Figure 6. Truss Actuator - Supporting Electrical Hardware

where **I** represents the identity matrix. The uncontrolled open-loop eigenvalues are shown in Table 2.

i	λ_i
1	0.000E+0 + 0.000E+0 i
2	0.000E+0 + 0.000E+0 i
3	0.000E+0 + 0.000E+0 i
4	-2.297E+5 + 0.000E+0 i
5	-5.937E+4 + 0.000E+0 i
6	-2.003E+4 + 0.000E+0 i
7	-1.707E-4 + 6.863E+1 i
8	-1.707E-4 - 6.863E+1 i
9	-1.292E-5 + 3.911E+0 i
10	-1.292E-5 - 3.911E+0 i
11	-7.123E-5 + 2.450E+1 i
12	-7.123E-5 - 2.450E+1 i

Table 2. Truss Actuator Open-loop Eignevalues

Note that the complex eigenvalue pairs: [9,10], [11,12] and [7,8] represent the first three modeled modes of a cantilevered beam respectively. They correspond to: 0.6225 Hz, 3.899 Hz and 10.923 Hz. Figures 7a and 7b show the experimental actuators root strain for uncontrolled first and second mode excitations of the beam. Third mode is not shown specifically, due to difficulty in its excitation, however its effect can be seen in the early response of second mode. By inference from Fig. 7, it can be shown that the actual first and second beam modes are 0.58 Hz and 3.80 Hz respectively; in close agreement with the model. Note here also that there is some structural damping inherent in the beam, especially in second and third modes. This unmodeled damping is neglected for the purposes of this research.

An aside about the separate modeling technique (actuator and beam) is appropriate here. Consider an assembly of the beam equations (Eq. 2.26) independent of the actuator. The first (lowest imaginary components) two complex eigenvalues closely resemble the first two modes for a free-free beam. It is believed that since the beam is modeled in free-space (with only coordinate references to ground) the beam model assembles the cantilevered modal shape functions to approximate a

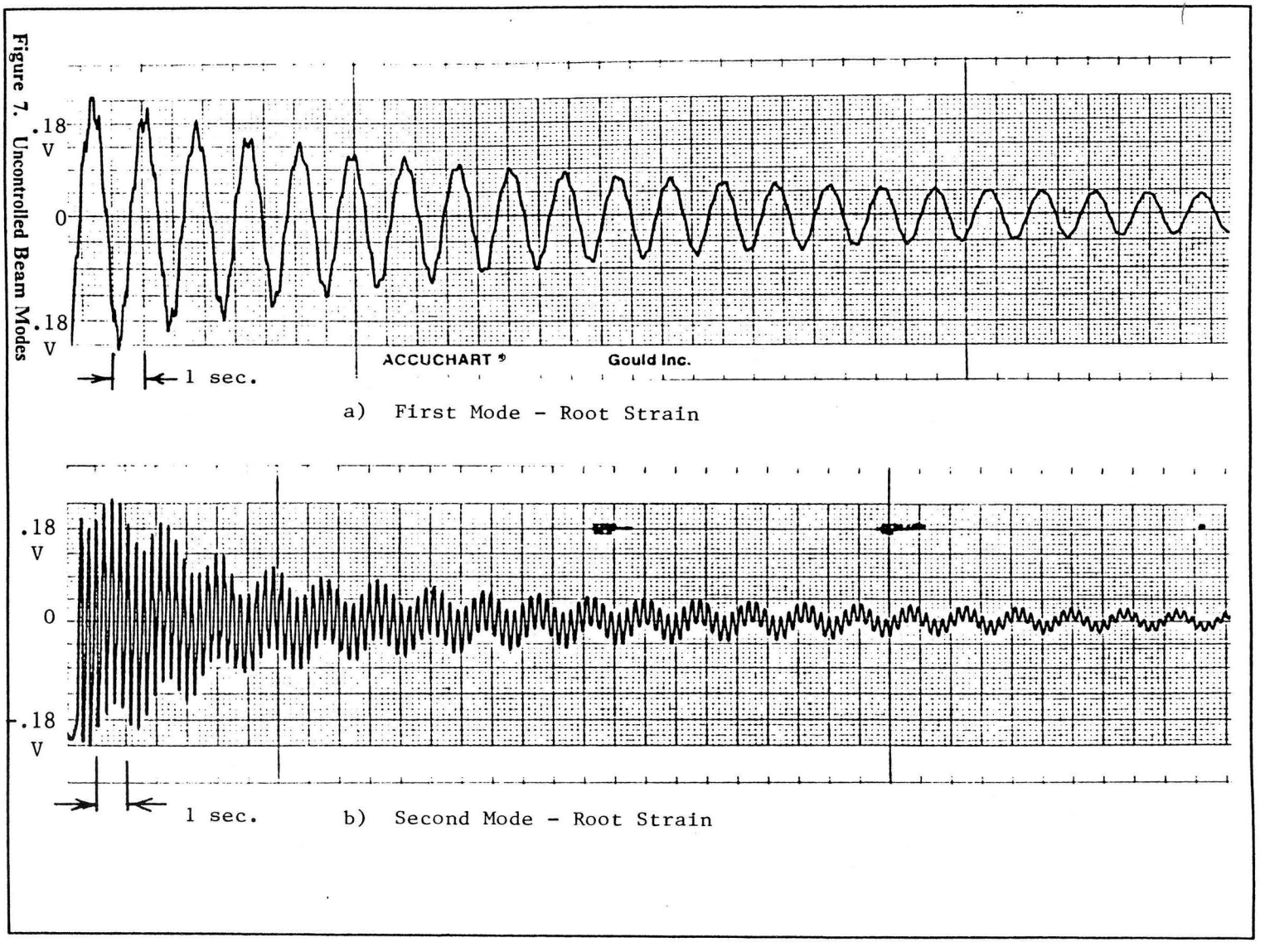

Figure 7. Uncontrolled Beam Modes

beam in free space (ie. free-free condition). Table 3 compares expected theoretical modes with those returned in the model.

	fundamental(Hz)	2nd mode (Hz)	3rd mode (Hz)
Modeled modes			
entire truss	0.6225	3.899	10.923
beam only	3.9736	10.9814	43.933
Theoretical modes (15)			
cantilevered	0.6244	3.9027	10.945
free-free	3.9736	10.945	21.465

Table 3. Comparison of modeled and expected modes

The remaining six system eigenvalues can be considered actuator eigenvalues. Note that three are at the origin in the s-plane while the others have only very large negative real components, indicating very fast response. This wide variation in open-loop pole placement is termed a "stiff" system. This stiff response can be credited to the derivation of the actuator equations (Eq. 2.16). The modeling accounts only for mass and damping elements with no energy storage mechanisms (springs). Therefore, three solutions to the set of actuator equations are trivial, (at the origin) and the other three are first-order. Although, exact measurement of the actuators speed of response was not possible due to instrumentation limitations, verification was made that its time constant, τ, was less than 0.008 sec, lending credibility to the stiff model.

It should also be noted here that the eigenvalues associated with the beam ($\lambda_7 - \lambda_{12}$) have very little damping. It has been shown (16) that if a more massive structure is attached to the actuator, greater damping is introduced in the beam due to the back EMF characteristics of the motor. In other words, only massive structures attached to the actuator have the ability to drive the actuator. This characteristic can also be attributed to the stiff model. Next, a transformation necessary for application of the Kalman gain sets will be derived.

4.3 The Gain Set Transformation Matrix

Section 4.2 describes the assembly of the system equations and a transformation to state space format. For convenience in experimentation, a change of variables is now introduced. The state vector is presented for reference:

$$\mathbf{x} = \begin{bmatrix} \mathbf{Pr} \\ \mathbf{q} \\ \dot{\mathbf{Pr}} \\ \dot{\mathbf{q}} \end{bmatrix} \qquad [4.3]$$

where $\mathbf{q}$ represents the vector of modal displacement coordinates. Note that $\mathbf{x}$ can be written as:

$$\mathbf{x} = \mathbf{x}_0 + \delta\mathbf{x} \qquad [4.4]$$

where $\mathbf{x}_0$ represents the systems "set point" and $\delta\mathbf{x}$ represents small displacements about that point. Since the only non-zero values in the set point vector are those introduced by $\mathbf{Pr}_0$ (see Appendix A), a substitution into the state space format described in Eq. 3.1 shows that the system equations can equivalently be written as:

$$\delta\dot{\mathbf{x}} = \mathbf{a}\,\delta\mathbf{x} + \mathbf{b}\,\mathbf{V} \qquad [4.5]$$

Chapter 3 describes a method for determining gains for full state feedback of any linear system. Application of the Kalman gain set (Eq. 3.4) requires multiplication by the state vector $\delta\mathbf{x}$. Actual measurement of these coordinates, however is difficult. As mentioned previously, the experimental actuator is equipped with linear potentiometers allowing measurement of the $\delta\mathbf{l}$ vector. In addition, the beam is instrumented with strain gages from which the modal displacement coordinates can be inferred. Therefore, the vector of measurable states is:

$$\delta\mathbf{x}' = \begin{bmatrix} \mathbf{E} \\ \boldsymbol{\varepsilon} \\ \dot{\mathbf{E}} \\ \dot{\boldsymbol{\varepsilon}} \end{bmatrix} \qquad [4.6]$$

where E_1, E_2, and E_3 represent the voltage output of the linear potentiometers. Similarly, $\boldsymbol{\varepsilon}$ represents the vector of voltage outputs from the strain gage bridge amplifiers. A "gain set transformation" (**D**) is necessary then such that:

$$\delta\mathbf{x} = \mathbf{D}\,\delta\mathbf{x}' \qquad [4.7]$$

The transformations from **E** to **Pr**-coordinates follow easily from Eqs. 2.5 and 2.6 assuming small deflections. A transformation from strain readings to modal displacement coordinates must then be found. Appendix C presents an empirical transformation of the form:

$$\mathbf{q} = \mathbf{f}\,\boldsymbol{\varepsilon} \qquad [4.8]$$

where **f** is the strain transition matrix. It can then be shown that:

$$\mathbf{D} = \begin{bmatrix} \dfrac{\mathbf{T}_l^{-1}}{G_p} & & & \\ & \mathbf{f} & & \\ & & \dfrac{\mathbf{T}_l^{-1}}{G_p} & \\ & & & \mathbf{f} \end{bmatrix} \qquad [4.9]$$

Therefore, Eq. 3.4 can be replaced by:

$$\mathbf{V} = -\mathbf{F}\,\mathbf{D}\,\delta\mathbf{x}' \qquad [4.10]$$

Next, two Kalman gain sets will be found and applied to the experimental truss actuator.

4.4 Kalman Gains Sets Determination and Application

Chapter 3 presents the time-invariant optimal control law to be used for control of the truss actuator. Two sets of these gains will now be applied to the experimental system. Selected time responses of system variables are presented.

4.4.1 Gain Set 1

According to Eq. 3.3 the penalty matrices on the state and control, **Q** and **R** , are chosen heuristically by eigenvalue placement as:

$$\mathbf{Q}_1 = [3\cdot 10^4 \quad 3\cdot 10^4 \quad 3\cdot 10^4 \quad 1.25\cdot 10^6 \quad 5\cdot 10^6 \quad 5\cdot 10^6 \quad 0 \quad 0 \quad 0 \quad 0 \quad 0 \quad 0]_D$$

$$\mathbf{R}_1 = [5 \quad 5 \quad 5]_D$$

where the *D* subscript indicates the vector elements represent the diagonal of a square matrix. Note that the beam's displacement is penalized heavily compared to the actuators displacement and the control is virtually non-penalized. Solving for the state feedback matrix **F**:

$$\mathbf{F}_1 = \begin{bmatrix} -1.69E+0 & 4.03E+1 & -6.61E+1 & 4.66E+2 & -7.96E+2 & 7.16E+2 \\ 6.92E+1 & 3.06E+1 & 1.68E+1 & 1.76E+2 & -5.64E+2 & 6.42E+2 \ \ldots \\ -3.49E+1 & 5.87E+1 & 3.66E+1 & -1.72E+1 & 2.04E+2 & -2.74E+2 \end{bmatrix}$$

$$\begin{bmatrix} 1.31E+1 & 1.91E-2 & -8.45E+0 & -6.89E+0 & 2.45E+0 & -4.53E-1 \\ \ldots\ 3.34E+0 & 7.21E-3 & -2.01E+0 & -1.58E+0 & 8.66E-1 & -2.03E-1 \\ 2.64E+0 & 7.41E-4 & -1.96E+0 & -1.70E+0 & 1.61E-3 & 2.36E-2 \end{bmatrix}$$

An examination of the above gains shows clearly that the feedback gains placed on velocities are significantly smaller than those on position. This is believed to be due to the fact that no penalties have been placed on velocities in the **Q** matrix. A further investigation shows that the velocity feedback can be removed entirely without significant change in closed-loop eigenvalues. As yet, this phenomen is unexplained. It will, however, be used in the control scheme to allow removal of velocity feedback. The actual feedback control matrix is then written as:

$$\mathbf{F'}_1 = \begin{bmatrix} -1.69E+0 & 4.03E+1 & -6.61E+1 & 4.66E+2 & -7.96E+2 & 7.16E+2 \\ 6.92E+1 & 3.06E+1 & 1.68E+1 & 1.76E+2 & -5.64E+2 & 6.42E+2 \ \ldots \\ -3.49E+1 & 5.87E+1 & 3.66E+1 & -1.72E+1 & 2.04E+2 & -2.74E+2 \end{bmatrix}$$

$$\begin{bmatrix} 0 & 0 & 0 & 0 & 0 & 0 \\ \ldots\ 0 & 0 & 0 & 0 & 0 & 0 \\ 0 & 0 & 0 & 0 & 0 & 0 \end{bmatrix}$$

The above gain set is then implemented on the analog computer. Figure 8 shows the wiring diagram used for this gain set. Note that the triangular shaped devices are DC amplifiers, and the number at the input of each represents a gain. The round devices are potentiometers and the number written next to each represents its attenuation. The "soft limiter" (17) is an external circuit that works in conjunction with several amplifiers. It is tuned to limit voltage output of the amplifiers to approximately ± 9 volts, thereby preventing overload of the analog computer driver amplifiers or the motor power amplifiers. A shorthand notation is used in Fig. 8 to show various

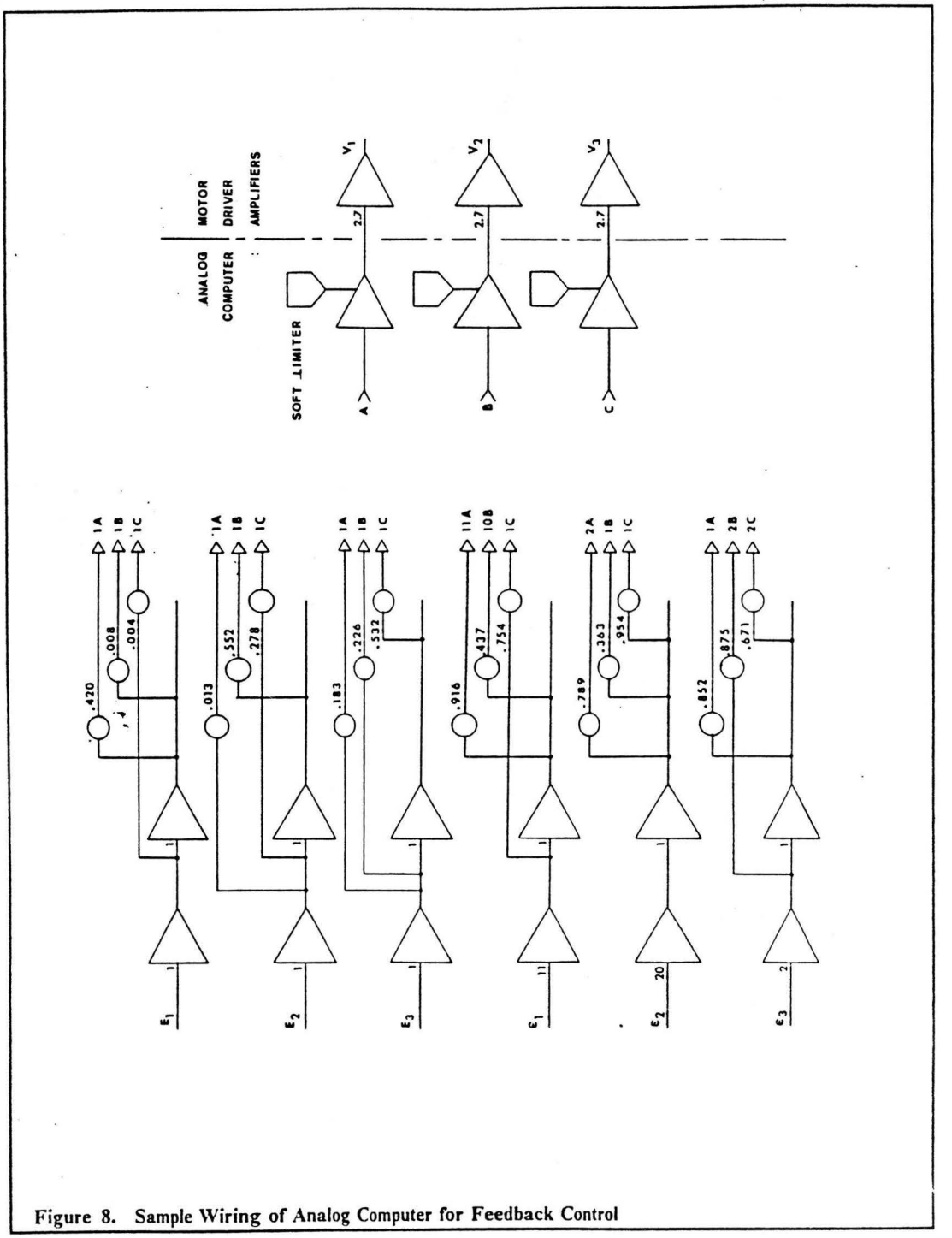

Figure 8. Sample Wiring of Analog Computer for Feedback Control

circuit connections. For example, a connection point (marked with an arrow) and the note "11A" represents a connection to an 11 gain input of the amplifier marked "A".

Figures 9 - 12 show root strain and control voltages for "first" and "second" mode excitations of the beam. The beam was bent into an approximate deflection for each mode. As the beam was released the systems feedback control was turned on. The effect of the soft limiters can clearly be seen in the **V** outputs.

4.4.2 Gain Set 2

Again, **Q** and **R** are chosen heuristically, based on the desire for a more dominant control than that presented with gain set 1 and the knowledge of realizable gains. They are presented as:

$$\mathbf{Q}_2 = [6\cdot 10^6 \quad 6\cdot 10^5 \quad 6\cdot 10^5 \quad 6.25\cdot 10^6 \quad 2.5\cdot 10^7 \quad 2.5\cdot 10^7 \quad 0 \quad 0 \quad 0 \quad 0 \quad 0 \quad 0]_D$$

$$\mathbf{R}_2 = [5 \quad 5 \quad 5]_D$$

The corresponding feedback matrix is then:

$$\mathbf{F}_2 = \begin{bmatrix} 4.69E+0 & 1.72E+2 & -3.00E+2 & 1.01E+3 & -1.75E+3 & 1.59E+3 \\ 3.11E+2 & 1.29E+2 & 7.86E+1 & 3.88E+2 & -1.26E+3 & 1.43E+3 \\ -1.51E+2 & 2.71E+2 & 1.53E+2 & -5.51E+1 & 4.63E+2 & -6.13E+2 \end{bmatrix} \ldots$$

$$\begin{bmatrix} 1.11E+2 & 5.01E-2 & -7.48E+1 & -6.24E+1 & 1.35E+1 & -2.66E+0 \\ 2.77E+1 & 1.71E-2 & -1.80E+1 & -1.48E+1 & 4.69E+0 & -1.13E+0 \\ 2.39E+1 & 5.88E-3 & -1.76E+1 & -1.52E+1 & 2.71E-1 & 5.35E-2 \end{bmatrix}$$

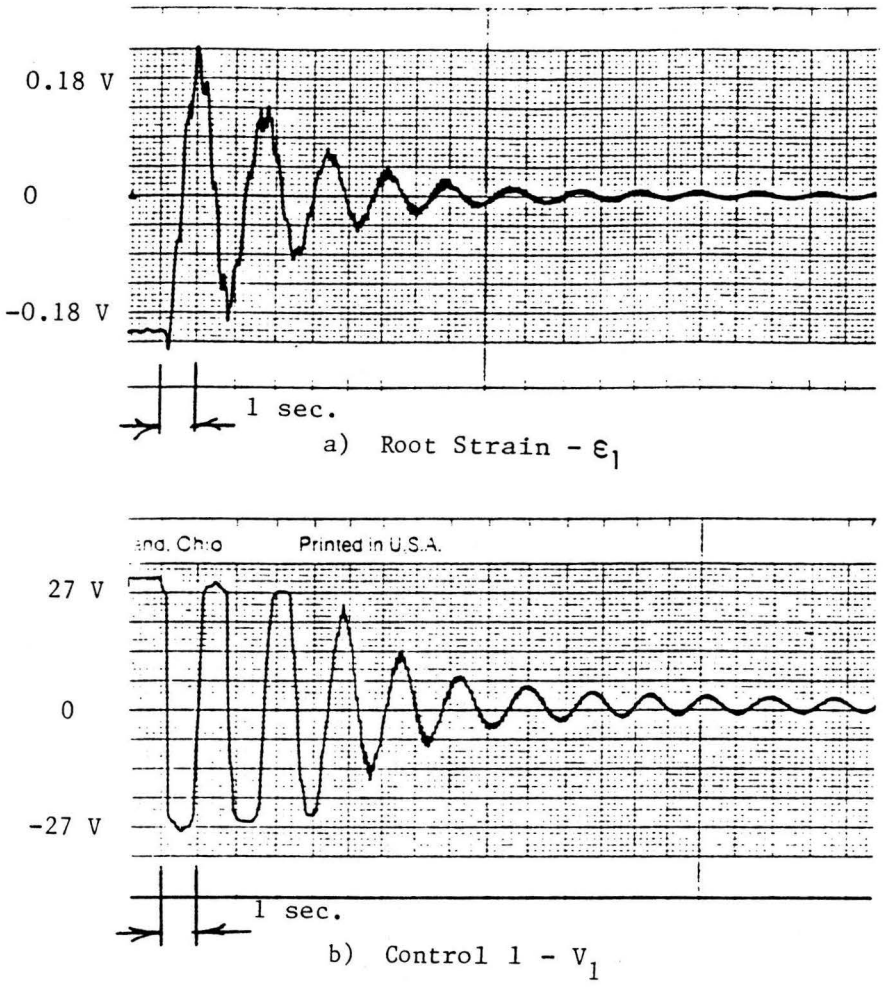

Figure 9. Controlled Responses to "First" Mode excitation: (Root Strain and Control Voltage) Gain Set 1

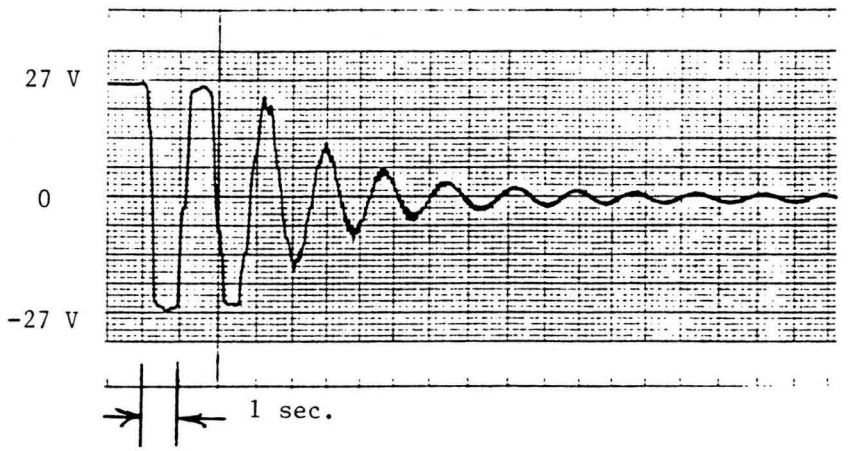

a) Control 2 - V_2

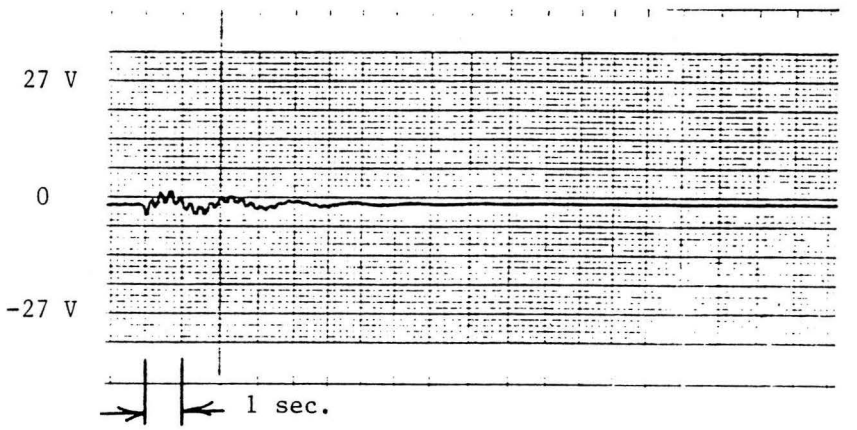

b) Control 3 - V_3

Figure 10. Controlled Responses to "First" Mode excitation: (Control Voltages) Gain Set 1

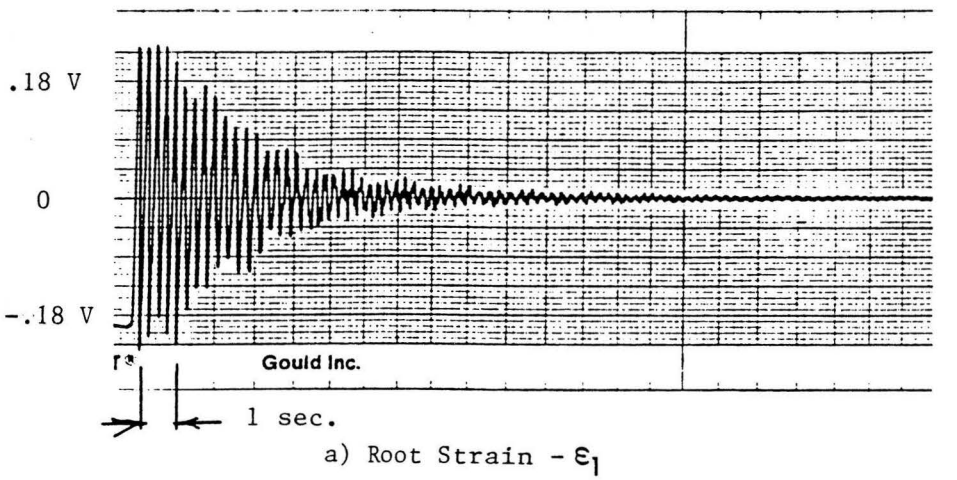

a) Root Strain - ε_1

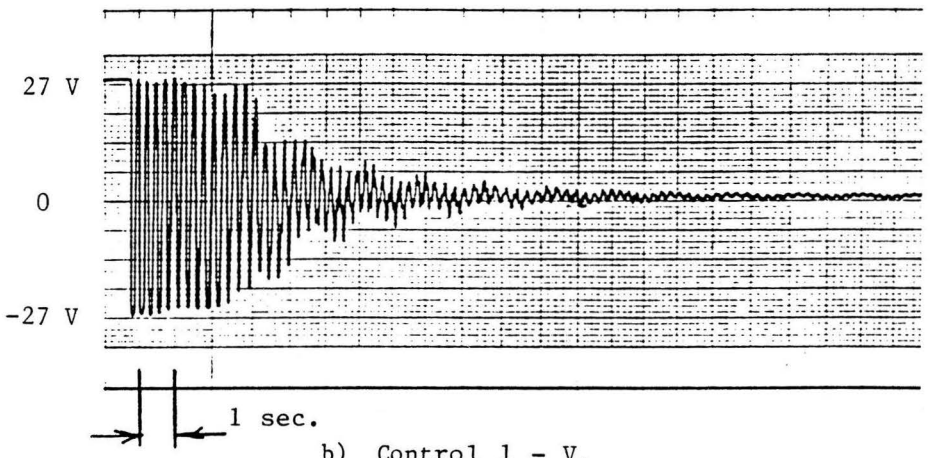

b) Control 1 - V_1

Figure 11. **Controlled Responses to "Second" Mode excitation:** (Root Strain and Control Voltage) Gain Set 1

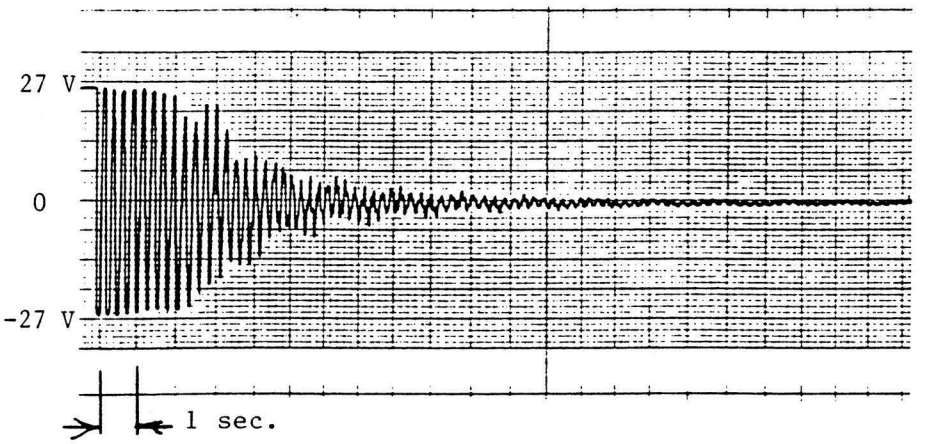

a) Control 2 - V_2

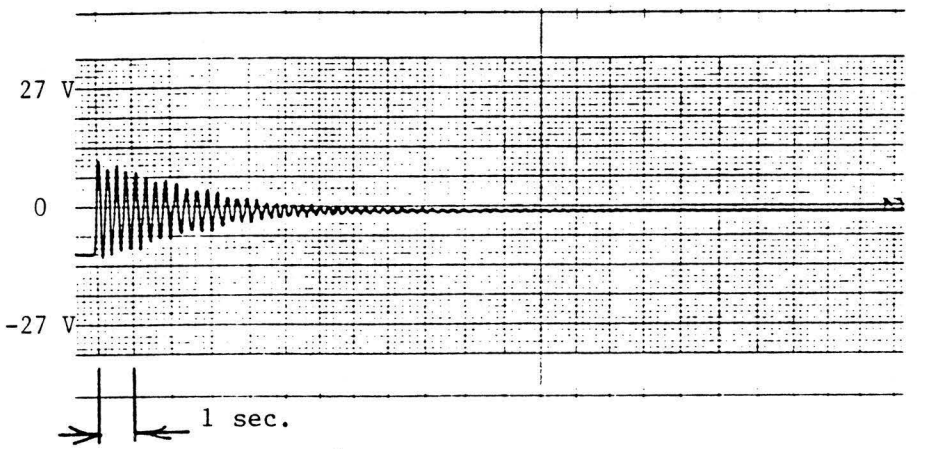

b) Control 3 - V_3

Figure 12. Controlled Responses to "Second" Mode excitation: (Control Voltages) Gain Set 1

$\mathbf{F'}_2$ is then found as before: by setting the velocity feedback terms (the right half of the above matrix) to zero. This gain set is also programmed on the analog computer. Representative time responses of root strain and control voltages are shown in Figs. 13-16.

Next, the responses presented in Figs. 9-16 will be discussed and compared with expected theoretical responses.

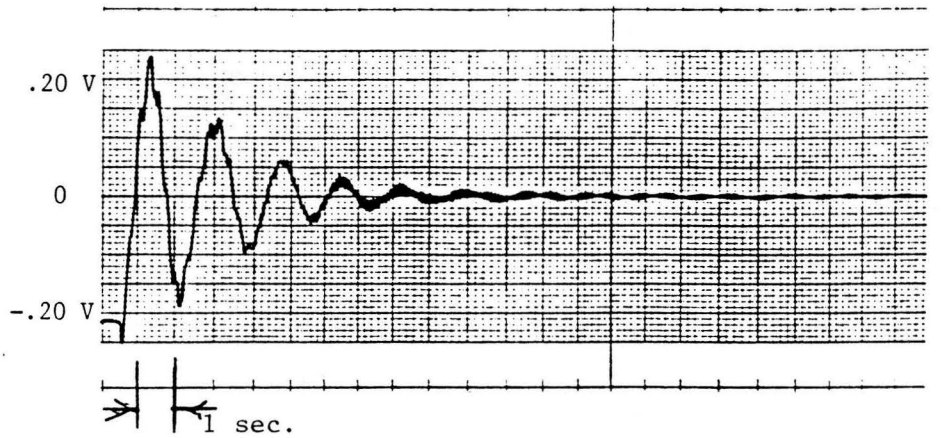

a) Root Strain - ε_1

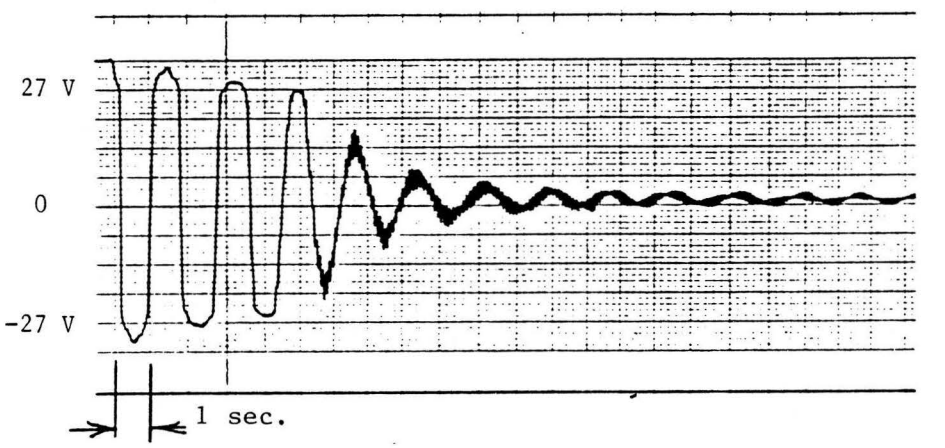

b) Control 1 - V_1

Figure 13. Controlled Responses to "First" Mode excitation: (Root Strain and Control Voltage) Gain Set 2

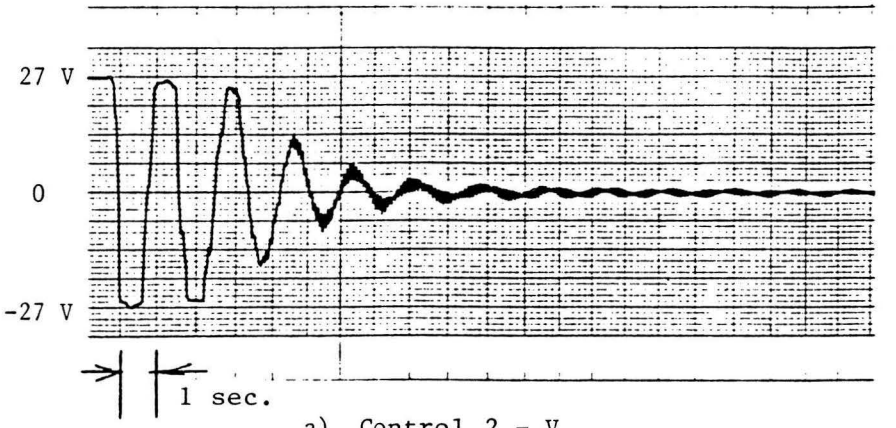

a) Control 2 - V_2

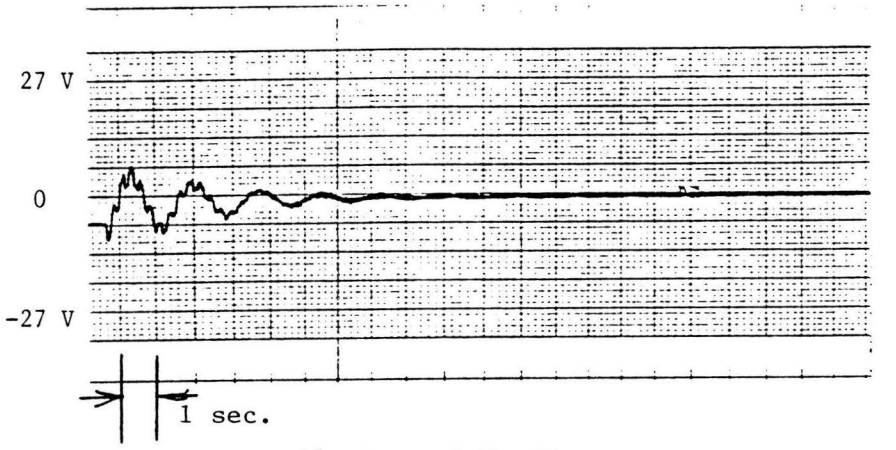

b) Control 3 - V_3

Figure 14. Controlled Responses to "First" Mode excitation: (Control Voltages) Gain Set 2

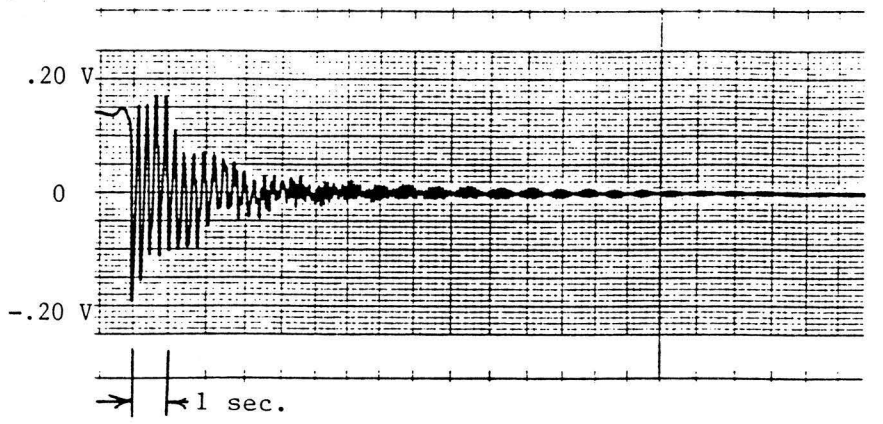

a) Root Strain - ε_1

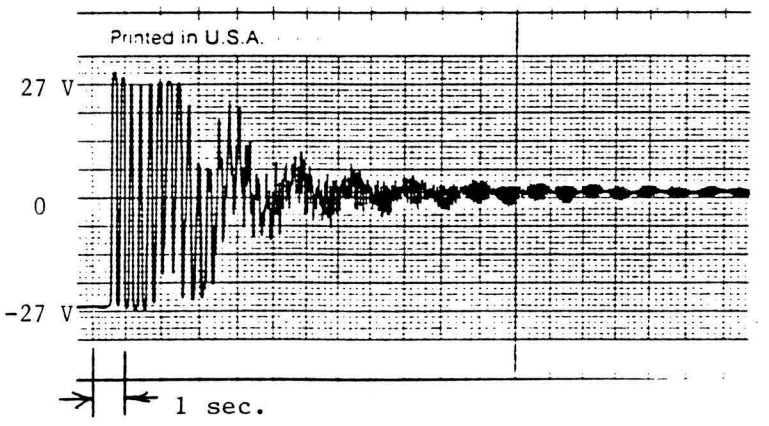

b) Control 1 - V_1

Figure 15. Controlled Responses to "Second" Mode excitation: (Root Strain and Control Voltage) Gain Set 2

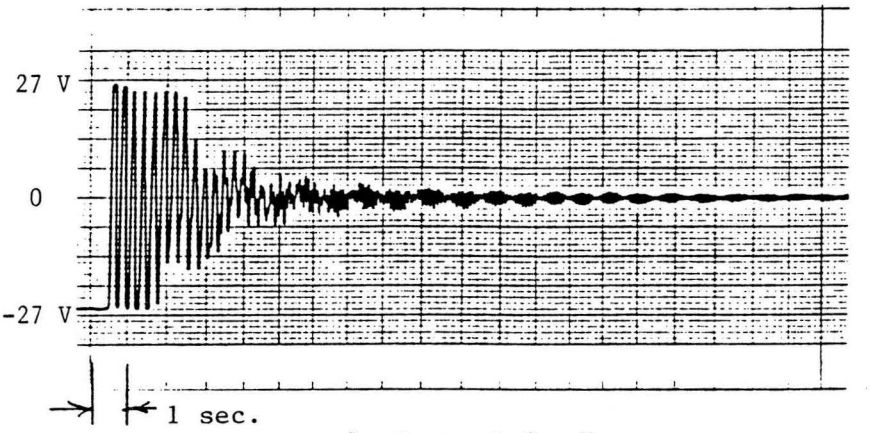

a) Control 2 - V_2

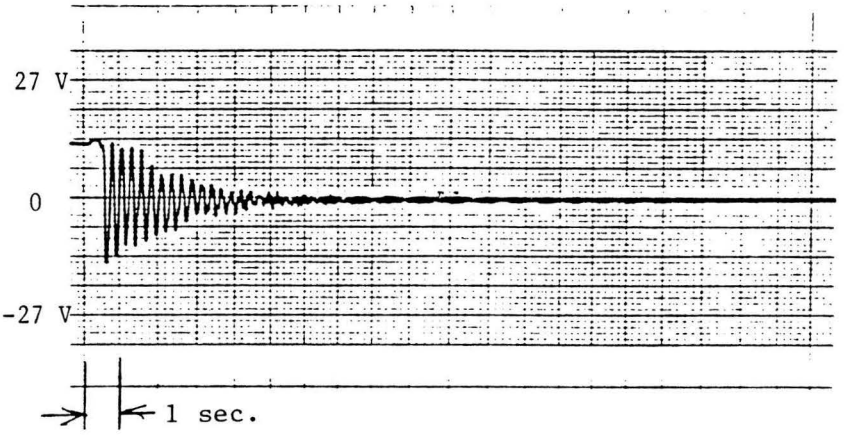

b) Control 3 - V_3

Figure 16. Controlled Responses to "Second" Mode excitation: (Control Voltages) Gain Set 2

5.0 Comparison of Results: Theoretical vs. Experimental

5.1 Introduction

This chapter will present a comparison of theoretical and experimental results. Since the primary goal of the truss actuator is to provide active damping of the attached flexible structure, the damping ratio will be used as a measure of effectiveness. The following sections will display the method of determining the experimental and theoretical damping ratios and present the results. A comparison and interpretation will then follow.

5.2 Calculations Summary

5.2.1 Theoretical

The method of determining the effective damping ratio for a modeled system begins with finding the eigenvalues for the controlled system similarly to Eq. 4.2:

$$(\mathbf{a} + \mathbf{b}\,\mathbf{F}'_i - \lambda\,\mathbf{I})\,\mathbf{x} = \mathbf{0} \qquad [5.1]$$

Since the apparent damping ratio of the beam is to be used as a measure of the actuators effectiveness, the eignevalues associated with the beam are selected. The damping ratio corresponding with each eigenvalue can then be found by:

$$\zeta = \frac{|\,\text{real}\,(\lambda)\,|}{\|\lambda\|} \qquad [5.2]$$

5.2.2 Experimental

The effective experimental damping ratio is computed by logarithmic decrement (18) from the controlled and uncontrolled time histories of root strain presented in chapter 4.

$$\zeta \cong \frac{1}{2\pi n} \ln\left[\frac{x_1}{x_n}\right] \qquad [5.3]$$

where the expression in brackets represents the ratio of amplitudes over n cycles. This approximation is valid for values of $\zeta < 0.4$.

The reduced data for effective controlled and uncontrolled beam damping is presented in the following table:

	Uncontrolled	Controlled gain set 1	Controlled gain set 2
Theoretical			
1st Mode	0.000	0.186	0.414
2nd Mode	0.000	0.014	0.031
Experimental			
1st Mode	0.020	0.091	0.110
2nd Mode	0.008	0.024	0.018

Table 4. Experimental vs. Analytical Structural Damping Ratios

5.3 Comparison and Discussion of Results

This section will provide a qualitative and quantitative analysis of the actuator's performance based on the effective structural damping analysis presented above, and the system's time responses presented in Chapter 4.

Referring to Table 4, it can be seen that the actuator is more effective, theoretically, in controlling first mode excitations of the beam than higher modes. This is true for both gain sets even though the **Q** weighting matrices for each apply a greater penalty to second mode vibrations. The experimental results confirm this. Several explanations for this exist including an ineffective choice for **Q**. Perhaps an even greater penalty must be placed on second mode vibration to effectively control it. Another possible contributor to the poor control of second mode is the relatively small pitch in each actuator link lead screw. A greater lead would allow faster actuator motions and better authority over higher modes.

It is also apparent in Table 4 that the experimental results compare more closely to theoretical in gain set 1 than 2. The most likely explanation for this is the higher gains involved. The higher voltage control signals are clipped by the soft-limiting circuit. This degrades the systems performance. Several other explanations for the discrepancies in analytical and experimental results are:

- System Non-Linearities: Both the model and the experimental actuator are have inherent non-linearities. The coordinate transformations introduced in the modeling technique and the determination of the feedback transformation matrix account for most analytical non-linearities. In addition, the soft-limiting within the control loop necessary to prevent overload of the analog amplifiers introduces a dominant non-linearity. Note that the optimal control

law utilized assumes unbounded control capabilities. Since this is never physically realizable, a different control approach is the only way to circumvent this problem.

- Another severe actuator non-linearity is caused by the installed motors on the actuator. The motors have an effective deadband of approximately 2.5 volts. Additionally, they are geared internally, introducing another non-linearity: backlash. Therefore, control of small displacements, using small control voltage, has poor effectiveness. Probably the most obvious solution to this problem is to use higher quality motors.

- Probably the most obvious non-linearity is apparent in the time responses using gain set 2. Note (Figs. 13a and 15a) that near the end of control the beam picks up a higher frequency vibration. Clearly this is being amplified in the control signal. Observation of the beam shows this to be a torsional vibration of the beam. Several factors contribute to this torsional beam excitation including:

  Beam Warp: The experimental beam is not completely straight. This effect is multiplied by the gravity field. When the beam reaches its maximum in vibrational excursion, it tends to roll into a torsional shape. This effect could be eliminated.

  Non-Ideal Strain Gage Placement: Since a strain gage must have some physical dimension, it is impossible to mount one that only measures strain on the neutral axis, any torsional vibration will be interpreted by the control law as a bending vibrational mode. In addition, several of the mounted gages are not centered on the neutral axis, amplifying the above effect.

Lack of Actuator Rigidity: Although the actuator is constructed almost entirely of aluminum (relatively stiff), it does have a certain amount of play to it. This is introduced primarily at the actuators pivot points by the bearings and the weakened link rigidity due to the lead screw mounting arrangement. Another lack of rigidity is introduced by the beam's mounting bracket. Each of these rigidity problems can reduced by more careful design.

6.0 Conclusions and Recommendations

Control of a flexible structure has been demonstrated. Preliminary experimental and analytical analysis has shown than the control actuator is much more effective at controlling low frequency (vs. high frequency) vibrations. Good experimental validation has been obtained for one gain set applied to the planer truss. The second gain set provided only fair agreement with theory due primarily to amplifier clipping limitations.

With these conclusions in mind, the following suggestions for further study are made:

- In-depth study of **Q** and **R** effects: The gain sets presented here are only first attempts at demonstrating effective control using a truss actuator. It is believed that more judicious selection of the gain weighting matrices can provide greater control authority over higher frequency structural vibrations than demonstrated here.

- Investigation of position only feedback phenomenon: Chapter 4 describes an unexplained phenomenon as a result of the **Q** and **R** matrix selection. Specifically, if velocity terms are left unpenalized in the **Q** matrix, velocity feedback can be removed from the control loop without significant degradation of control. This effect should be investigated for some mathematical justification.

- Application of velocity feedback: The above mentioned phenomenon should be investigated experimentally by application of the velocity feedback terms to the control loop. In addition, velocity penalty terms should be used in the optimal gain selection weighting matrices.

- Full bi-linearization of the Lagrangian: The system equations presented in chapter 2 are linearized at several points, primarily for convenience. A more standard approach to linearization in the derivation is bi-linearization. The Lagrangian is first written in its full non-linear form, and then linearized by forming a quadratic Taylor expansion about the chosen operating point. This linearization will not affect the ability to model the beam and truss separately. It is believed by this experimenter that model differences introduced by the bi-linearization (as compared with the model presented here) will be minor if existent at all. It should be investigated however.

- Digital Control: Since the ultimate goal of this research is extension to a three dimensional actuator(s), digital control is a necessary step. In addition to providing a more physically compact controller (necessary in space), computers provide much greater numerical processing capabilities than that provided by the analog computers used here. Although digital control introduces an entirely new set of control problems, they must be solved if a large and kinematically complex structure is to be controlled.

- Investigate effects of model parameter changes: The experimental truss has a great many variables including motor parameters (gear ratio, back-emf coefficient, torque constant etc.), set point ($\mathbf{Pr}_0$), lead screw gain and number of modeled modes. All have the ability to significantly affect the control capabilities of the actuator and should be investigated.

- Extension to 3-D: This is the final goal of the actuator for application in space.

In conclusion, good control ability has been shown for low frequency vibrations. The truss actuator concept of integrating the control actuator within the controlled structure then provides a significant hope. Clearly, though work has just begun on proving a truss actuator capable of providing effective control for large space structures.

Bibliography

1. Fontana, A., and Hanks, B.R., "Control of Flexible Structures (COFS) Flight Experiment Program," *Proceedings of the 5th VPI and SU/AIAA Symposium on Dynamics and Control of Large Flexible Space Structures*, edited by L. Meirovitch, 1985.

2. Kosut, R.L., Salzwedel, H. and Emami-Naeini, A., "Robust control of Flexible Spacecraft," *Journal of Guidance and Control*, March - April 1983, pp. 104-111.

3. Nurre, G.S., Ryan, R.S., Scofield, H.N. and Sims, J.L., "Dynamics and Control of Large Space Structures," *Journal of Guidance and Control*, Sept. - Oct. 1984, pp. 514-526.

4. McClamroch, N.H., "Vibration Control of Flexible Structures using Member Dampers," *Proceedings of the 24th Conference on Decision and Control*, Ft. Lauderdale, Fl., December 1985.

5. Johnson, C.R., Jr., "Adaptive Modal Control of Large Flexible Spacecraft," *Journal of Guidance and Control,* July - Aug. 1980, pp. 369-375.

6. Mills, R.A., "Active Vibration Control of a Cantilevered Beam: A Study of Control Actuators," *Proceedings of the 34th Congress of the International Astronautical Federation.* Budapest, Hungary, October 1983.

7. Zimmerman, D.C., Horner, G.C. and Inman, D.J., "Microprocessor Controlled Force Actuator," Submitted to: *Journal of Guidance and Control.*

8. Juang, J.-N., Horta, L.G. and Robertshaw, H.H., "A Slewing Control Experiment for Flexible Structures," *Journal of Guidance and Control*, Sept. - Oct. 1986, pp. 599-607.

9. Major, C.S., and Simonian, S.S., "An Experiment to Demonstrate Active and Passive Control of a Flexible Structure," *Proceedings of the American Controls Conference*, San Diego, Ca., June 1984.

10. Opdenacker, Ph.C., Jonckheere, E.A., and Safonov, M.G., "Reduced Order Compensator Design for an Experimental Large Flexible Structure," *Proceedings of the 24th Conference on Decision and Control*, Ft. Lauderdale, Fl., December 1985.

11. Meirovitch, L., *Methods of Analytical Mechanics*, McGraw-Hill, New York, NY, 1970.

12. Kirk, D.E., *Optimal Control Theory*, Prentice-Hall, Englewood Cliffs, N.J., 1970, pp. 209-218.

13. Kalman, R.E., "Contributions to the Theory of Optimal Control," *Bol. Soc. Mat. Mex.*, 1960, pp. 102-119.

14. Russel, D.L., *Mathematics of Finite Dimensional Control Systems*, Lecture Notes in Pure and Applied Mathematics, 43, Marcel Decker Inc., N.Y., (1979).

15. Thompson, W.T., *Theory of Vibration with Applications*, Prentice-Hall, Englewood Cliffs, N.J., 1981, pp. 218-221.

16. Lovejoy, V.D., Robertshaw, H.H., Patten, W.N., Horner, G.C., "Dynamics and Control of a Planar Truss Actuator," Submitted to: *ASME Journal of Vibration, Acoustics, Stress and Reliability in Design.*

17. Electronic Associates, Inc., *Handbook of Analog Computation*, EAI Publishing, 1967, pp. 372..

18. Hale, F.J., *Introduction to Control System Analysis and Design* Prentice-Hall, Englewood Cliffs, N.J., 1973, pp. 94-96.

Appendix A. Experimental Planar Truss Test Stand - Characteristics

- Motor Characteristics

  Manufacturer - Type: Airco 2360-2848 24 Volts DC

  Gear Ratio: 64:1

  Electrical Characteristics - Experimentally Determined:

  $K_t = 0.4237 \ \frac{N \cdot m}{Amp}$

  $K_b = 1.014 \ Volts \cdot \sec$

  $R_a = 1.10 \ \Omega$

- Motor Amplifiers

  Input Voltage Range: $\pm$ 10 Vdc

  Output Voltage Range: $\pm$ 27 Vdc

  Power Supply: Positive + 27 V, Negative - 27 V

  Amplifier Gain: 2.7

- Potentiometers

  Manufacturer - Type: Waters LFS - 12 - OAS

  Stroke: 12 in.

  Resistance: 5 $k\,\Omega$

  Voltage span: 20 Volts

Potentiometer gain: $G_p = 65.62 \frac{Volts}{m}$

- Ballscrews

  Manufacturer - Type: Rockford

  lead: $G = 8.0851 \cdot 10^{-4} \frac{m}{\text{rad}}$

- Beam

  Supplier - Associated Spring Inc.

  Steel - SAE 1075 Spring Steel

  Physical Characteristics - Measured / Computed

  thickness: $t = 7.874 \cdot 10^{-4}\ m$

  length: $l = 1.016\ m$

  height: $h = 0.1016\ m$

  mass/unit length: $\xi = 0.6245 \frac{kg}{m^3}$

  flexure rigidity: $EI = 0.8267\ N \cdot m^2$

  Beam Integrals

$$I_1 = \int_0^L \varphi_1(x)\,dx = 0.39794$$

$$I_2 = \int_0^L \varphi_2(x)\,dx = -0.22067$$

$$I_3 = \int_0^L \varphi_3(x)\,dx = 0.13131$$

$$I_4 = \int_0^L [\varphi_1(x)]^2\,dx = 0.25418$$

$$I_5 = \int_0^L [\varphi_2(x)]^2\,dx = 0.25379$$

$$I_6 = \int_0^L [\varphi_3(x)]^2 \, dx = 0.25506$$

$$I_7 = \int_0^L 2\,\varphi_1(x)\,\varphi_2(x)\,dx = -0.00061$$

$$I_8 = \int_0^L 2\,\varphi_1(x)\,\varphi_3(x)\,dx = 0.00341$$

$$I_9 = \int_0^L 2\,\varphi_2(x)\,\varphi_3(x)\,dx = 0.00226$$

$$I_{10} = \int_0^L \varphi_1(x)\,x\,dx = 0.29370$$

$$I_{11} = \int_0^L \varphi_2(x)\,x\,dx = -0.04711$$

$$I_{12} = \int_0^L \varphi_3(x)\,x\,dx = 0.01856$$

$$I_{13} = \int_0^L [\varphi''_1(x)]^2 \, dx = 2.93709$$

$$I_{14} = \int_0^L [\varphi''_2(x)]^2 \, dx = 115.1785$$

$$I_{15} = \int_0^L [\varphi''_3(x)]^2 \, dx = 907.5255$$

$$I_{16} = \int_0^L 2\,\varphi''_1(x)\,\varphi''_2\,dx = 0.09233$$

$$I_{17} = \int_0^L 2\,\varphi''_1(x)\,\varphi''_3\,dx = -0.45242$$

$$I_{18} = \int_0^L 2\,\varphi''_2(x)\,\varphi''_3\,dx = 4.80997$$

- Strain Gages

  Manufacturer - Type: Measurements Group, Inc. CEA-06-240UZ-120

  Resistance: 120.0 Ω

  Gage Factor: 2.05 *at* 75°

- Strain Gage Bridge Amplifiers

  Manufacturer - Type: Measurements Group, Inc. P-3500

- Analog Computers

  Manufacturer - Type: Electronics Associates Inc. TR-20

- Power Supplies

  Manufacturer - Type: Power-Mate Corp. OEM-36H-OV-P2373A

- Truss Actuator Physical Constants

i	$J_{i\varphi}$ ($kg \cdot m^2$)	J_{il} ($kg \cdot m^2$)	r_i (m)	m_i (kg)
1	1.038	3.94	0.602	2.476
2	5.590	2.49	0.155	3.920
3	1.038	3.94	0.602	2.476

$J_p = 0.475 \ kg \cdot m^2$

$M_p = 3.330 \ kg$

$\mathbf{Pr}_0 = [0.610\,m \quad 1.219\,m \quad 0.0\,\text{rad}]^t$

Appendix B. Planar Actuator Model

This appendix presents the set of specific equations governing the experimental planar truss actuator. Data given in appendix A is inserted into the equations of motion derived in chapter 2. The governing equation (2.27) is repeated here for reference:

$$[\, 2\,\mathbf{M}_b + \mathbf{M}_c \,]\,\ddot{\mathbf{y}} + \left[\frac{K_t\,K_b}{G^2\,R_a}\,\mathbf{T}_l^t\,\mathbf{T}_l\right]\dot{\mathbf{y}} + \mathbf{K}_c\,\mathbf{y} = \frac{K_t}{G\,R_a}\,\mathbf{T}_l^t\,\mathbf{V} \qquad [B.1]$$

The necessary transformations, $\mathbf{T}_l$ and $\mathbf{T}_\varphi$ are first formed according to Eqs. 2.5 and 2.8 using the data provided in appendix A for $\mathbf{Pr}_0$. $\mathbf{M}_b$ can then be formed according to Eq. 2.10. The remainder of the model generation then follows clearly from definitions presented in chapter 2. For simplicity, Eq. B.1 can now be expressed as:

$$\mathbf{M}\ddot{\mathbf{y}} + \mathbf{C}\dot{\mathbf{y}} + \mathbf{K}\mathbf{y} = \mathbf{B}\mathbf{V} \qquad [B.2]$$

where $\mathbf{M}$ =

$$\begin{bmatrix}
9.376E+0 & -1.270E+0 & -7.614E-1 & -2.485E-1 & 1.378E-1 & -8.199E-2 \\
-1.270E+0 & 1.533E+1 & 1.957E+0 & 0.000E+0 & 0.000E+0 & 0.000E+0 \\
-7.614E-1 & 1.957E+0 & 4.815E+0 & 1.834E-1 & -2.941E-2 & 1.159E-2 \\
-2.485E-1 & 0.000E+0 & 1.834E-1 & 1.587E-1 & -1.898E-4 & 1.065E-3 \\
1.378E-1 & 0.000E+0 & -2.941E-2 & -1.898E-4 & 1.586E-1 & 7.053E-4 \\
-8.199E-2 & 0.000E+0 & 1.159E-2 & 1.065E-3 & 7.053E-4 & 1.592E-1
\end{bmatrix}$$

$$\mathbf{C} = \begin{bmatrix}
8.195E+5 & 2.654E+5 & 3.754E+5 & 0.000E+0 & 0.000E+0 & 0.000E+0 \\
2.654E+5 & 7.085E+5 & 5.794E+5 & 0.000E+0 & 0.000E+0 & 0.000E+0 \\
3.754E+5 & 5.794E+5 & 8.195E+5 & 0.000E+0 & 0.000E+0 & 0.000E+0 \\
0.000E+0 & 0.000E+0 & 0.000E+0 & 0.000E+0 & 0.000E+0 & 0.000E+0 \\
0.000E+0 & 0.000E+0 & 0.000E+0 & 0.000E+0 & 0.000E+0 & 0.000E+0 \\
0.000E+0 & 0.000E+0 & 0.000E+0 & 0.000E+0 & 0.000E+0 & 0.000E+0
\end{bmatrix}$$

$$\mathbf{K} = \begin{bmatrix}
0.000E+0 & 0.000E+0 & 0.000E+0 & 0.000E+0 & 0.000E+0 & 0.000E+0 \\
0.000E+0 & 0.000E+0 & 0.000E+0 & 0.000E+0 & 0.000E+0 & 0.000E+0 \\
0.000E+0 & 0.000E+0 & 0.000E+0 & 0.000E+0 & 0.000E+0 & 0.000E+0 \\
0.000E+0 & 0.000E+0 & 0.000E+0 & 2.428E+0 & 3.816E-2 & -1.870E-1 \\
0.000E+0 & 0.000E+0 & 0.000E+0 & 3.816E-2 & 9.521E+1 & 1.988E+0 \\
0.000E+0 & 0.000E+0 & 0.000E+0 & -1.870E-1 & 1.988E+0 & 7.502E+2
\end{bmatrix}$$

$$\mathbf{B} = \begin{bmatrix}
0.000E+0 & 3.368E+2 & 0.000E+0 \\
4.764E+2 & 3.368E+2 & 4.764E+2 \\
-2.904E+2 & 2.053E+2 & 2.904E+2 \\
0.000E+0 & 0.000E+0 & 0.000E+0 \\
0.000E+0 & 0.000E+0 & 0.000E+0 \\
0.000E+0 & 0.000E+0 & 0.000E+0
\end{bmatrix}$$

Appendix C. Experimental Determination of Strain Transformation Matrix

The strain transition matrix, **f** described in chapter 4 was determined experimentally. The matrix provides a transition such that:

$$\mathbf{q} = \mathbf{f}\,\varepsilon \qquad [C.1]$$

where ε represents the vector of outputs from the strain guage amplifiers and **q** represents the vector of modal displacement coefficients. The above equation must first be inverted to determine **f**.

$$\varepsilon = \mathbf{f}^{-1}\,\mathbf{q} \qquad [C.2]$$

A set of three forms were made of wood to enable the experimenter to clamp and hold the beam in each of the three modeled modes. This permits the measurement of static strains. One such form is shown in Fig. 5. First, the beam was clamped into its first mode deflection with a + 0.1254 m end deflection. Each of the ouputs from the three strain guage amplifiers was then read. This process was then repeated for second and third modes, again assuring a + 0.1254 m end deflection. The results are presented in the following table.

	ε_1 (volts)	ε_2 (volts)	ε_3 (volts)
mode 1	+ 0.167	+ 0.025	- 0.025
mode 2	- 0.581	+ 0.050	+ 2.150
mode 3	+ 1.100	- 0.255	- 0.550

Table 5. Strain Readings for Modal Deflections

This data can then be substuited into Eq. C.2, one mode at a time since q is known for each data set as 0.1254 m. **f** is then found as:

$$\mathbf{f} = \begin{bmatrix} 0.5852 & 2.2986 & 0.1047 \\ 0.0226 & -0.0721 & 0.0787 \\ 0.0618 & -0.3864 & 0.0257 \end{bmatrix}$$

The vita has been removed from the scanned document